Rheology of Highly Filled Propylene/Ethylene Copolymers

Cheng Huang

A Thesis

in

The Department

of

Mechanical & Industrial Engineering

Presented in Partial Fulfillment of the Requirements

for the Degree of Master of Applied Science (Mechanical Engineering)

Concordia University

Montreal, Quebec, Canada

April 2006

Your file Votre référence
ISBN: 0-494-14307-X
Our file Notre référence
ISBN: 0-494-14307-X

Abstract

Rheology of Highly Filled Propylene/Ethylene Copolymers

Cheng Huang

Rheology of filled polymeric systems is an ever expanding area for industrial researchers. New experimental propylene-ethylene copolymers supplied by The Dow Chemical Company have a unique chain microstructure and an excellent balance of product performance properties. They feature narrow molecular weight distribution and broad crystallinity distribution. The unique molecular architecture offers the distinguishing feature of allowing exceptionally high filler loadings (even higher than 80wt %) yet maintaining good processability. Our goal is to thoroughly characterize the rheological behavior and the interfacial phenomena to provide a fundamental understanding of the lower than expected viscosity. Such a fundamental understanding is necessary for the design of other new resins with a better capacity for incorporating particles and for the development of optimum processing conditions for the composites.

In this work, the rheological properties of experimental P/E copolymers filled with calcium carbonate are studied. Steady shear and dynamic measurements on composites with different loadings (0-80 wt %) are carried out.

The steady state shear viscosity increases dramatically with increasing filler loading. To minimize/prevent bulk slip, rough plates are used for the samples with 80 wt% loading. The layer coated with calcium stearate decreases the adhesion of the polymer to the filler copolymers surface which results in particle-matrix interfacial slip. The ethylene-enriched zones are detected in the melt state, which causes the thermorheologically complex behavior and leads to a better particle dispersion.

Meanwhile the ethylene-enriched chains congregating preferentially on the particle surface under shear flow enhances particle-matrix interfacial slip.

The dynamic measurements indicate a time-dependent rheological behavior. Due to the particle motion, filled systems with different loadings and different interfacial interaction have different time dependency. With the increasing of filler loading, all the filled systems exhibit increasing complex viscosities. A critical volume fraction of 0.125 is predicted by a curve fitting. At low frequency, when the particle volume fraction is higher than 0.125, the filled polymer systems are elastically dominated. Due to the high loadings of particles, N-P/E and m-P/E with 60% loading are solid-like at low frequency.

Acknowledgements

I would like to express my sincere gratitude to my supervisor Prof. Paula M. Wood-Adams for her guidance and encouragement both in this work and in my life.

Special thanks go to my colleagues: Dr. Luminita, Ark and Yury (two nice Russian guys), Heng Wang, Wensheng Xu and Chongyu Wang (three Chinese guys), Ramin, Navid, Niyusha and Albortz (four Iranian people) for their help and useful discussions.

I would like to give my heartfelt thanks to Prof. John Dealy and his rheology group of Chemical Engineering Department of McGill University for their generous support. Special thanks to Prof. Marie-Claude Heuzey and her research associate Miss Mélina Hamdine in Chemical Engineering Department of École Polytechnique de Montréal for their help.

Thanks to Dr. Ming Xie of composite lab. He helped me a lot on laboratory facilities.

I would like to give my appreciation to The Dow Chemical Company and the National Science and Engineering Research Council of Canada (NSERC) for their funding of this project.

Finally, I would like to thank my wife and lovely daughter for their love, encouragement and support throughout my life.

Table of Contents

List of Figures

List of Tables

Chapter 1. Introduction

1.1 Metallocene Polyolefins

Polyolefins are the most used plastics in the world and are found in almost every area like food packaging, home appliances and engineering components. Polyolefins are considered to be "commodity polymers" which include polypropylene (PP), polyethylene (PE) and their copolymers with alpha olefins such as 1-butene, 1-hexene and 1-octene.

Before the arrival of the metallocene catalysts in the 1980s, most polyolefins were produced by Ziegler-Natta catalysts. The manufacture of polyolefins by metallocene catalysts represents a revolution in the polymer industry. The metallocene catalysts only allow olefin polymerization at a single site, whereas Ziegler-Natta catalysts have a range of active sites. This results in a better control of molecular structure and improved physical properties.

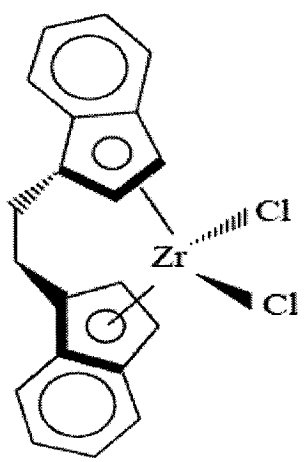

Figure 1.1 Chemical structure of a typical metallocene catalyst ($Et[Ind]_2ZrCl_2$)[1]

Usually the properties of polyolefins are dependent on their microstructures such as molecular weight distribution (MWD), branching structure, stereoregularity and chemical composition distribution (CCD). Metallocene polyolefins have relatively narrow molecular distribution (Mw/Mn=2-3) and improved strength, sealability, optical properties which makes them ideal for use as ultra-thin films.

1.2 New Propylene/Ethylene Copolymers based on Post-Metallocene Catalysts

Post-metallocene catalyst is the next generation of catalysts used for olefin polymerization. Since these catalysts are newly-designed and are proprietary, we can not provide additional information about the catalyst.

Usually single-site conventional metallocene catalysts ($Et[Ind]_2ZrCl_2$) can not be used for controlling molecular weight distribution. This behavior provided easy ways of controlling MWD of polyethylene produced with bimetallic supported catalysts, when $Et[Ind]_2ZrCl_2$ is combined with other metallocene catalysts [2]. Relatively, it is more difficult to control the chemical composition distribution than molecular weight distribution. In industry, reactor cascade technology combined with catalyst technology is used to control the CCD and MWD to produce a mixture of different polymers with different microstructures.

The family of propylene-ethylene (P/E) copolymers from The Dow Chemical Company based on post-metallocene catalysts and INSITE* Technology, have a unique chain microstructure and an excellent balance of product performance properties [3, 4, 5]. They feature narrow molecular weight distribution and broad crystallinity distribution. Figure 1.2 and Figure 1.3 [3] show the differences of the new P/E copolymers as compared to the traditional P/E copolymers. Temperature Rising Elution Fractionation

(TREF) has been known as the most effective method for polyolefin fractionation. These two figures below show the copolymer fractions with different comonomer distributions. Note that the new propylene/ethylene copolymer included in these figures is of the same family as the resin we have studied but not exactly the same.

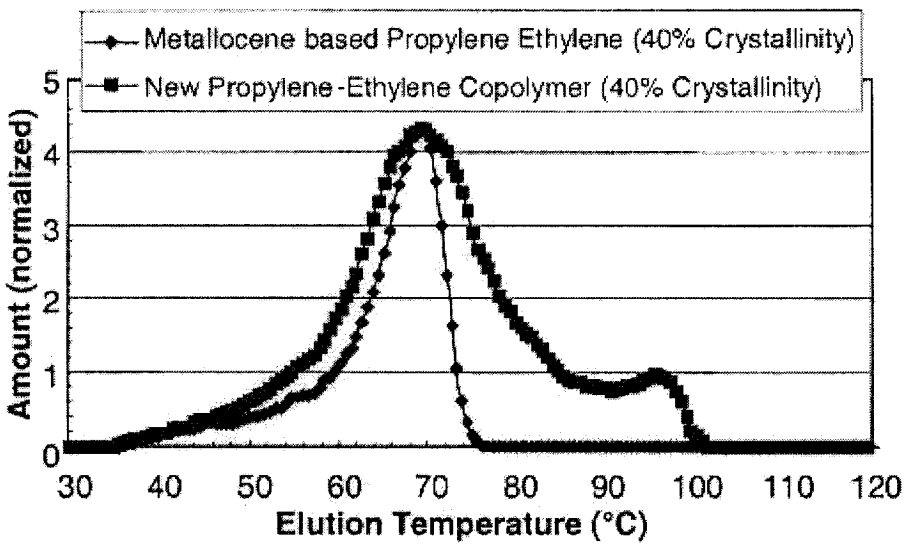

Figure1.2 Comonomer distributions of different P/E copolymers [3]

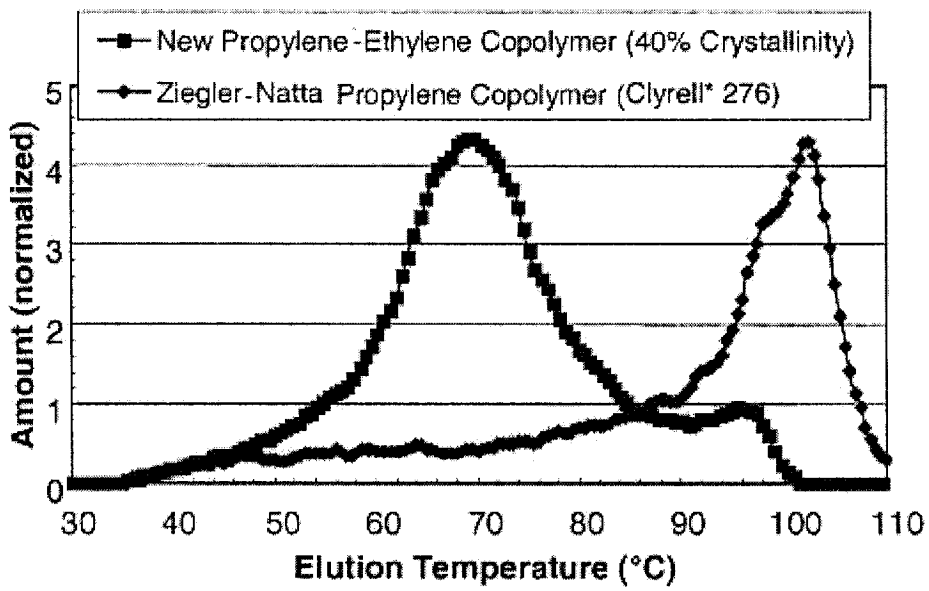

Figure 1.3 Comonomer distributions of different P/E copolymers [3]

The unique molecular architecture offers the distinguishing feature of allowing exceptionally high filler loadings yet maintaining good processability. This provides the potential for reduced material cost in highly filled compounds in, for example, wire and cable and for increased sound-deadening capability in noise vibration compounds. In this work, the rheological properties of highly $CaCO_3$-filled propylene-ethylene copolymers were studied. Industrial studies have demonstrated that these new P/E copolymers can incorporate extremely higher filler loadings (up to 80 wt %) and still remain processable.

Solid particles are frequently used in polymeric materials to improve their particular properties or impart to them the different properties of the solid, while retaining the processability of the molten polymer. The diverse properties of polymers and solid fillers determine the rheological behavior of the filled polymer melts and the maximum filler content. In this work, stearate-treated ultrafine calcium carbonate ($CaCO_3$) was used. $CaCO_3$ treated with an interfacial agent such as stearic acid or stearate is often used in place of untreated calcium carbonate to take advantage of improved lubricity and wetting characteristics. These characteristics typically lead to lower mixing viscosity, improved filler dispersion and better flow properties. Also due to the weak particle-matrix adhesion, the filled system is ideal for producing breathable film which is widely used in food packaging industry. Generally, the morphology of the wetting interface between the polymer and filler particles is studied in terms of contact angle, surface and interfacial tension and polarity.

Generally, the viscosity of a filled system is usually much higher than a non-filled system mainly due to the formation of filler aggregates. The aggregated filler shows a higher apparent filler fraction, ϕ_a, than the true filler fraction, ϕ, because the interstices

of the aggregates are not easily accessible to the resin. The viscosity is a nonlinear function of the filler fraction, and the viscosity increases much more rapidly at higher filler fractions, especially near the maximum packing fraction, ϕ_{max}. A drastic viscosity reduction of a highly filled system can be achieved by breaking up the aggregates of the filler. Another possible explanation for viscosity reduction in such a system is interfacial slip. The main objective of this project will be to explore the reasons for the low viscosity with high filler content both from the theoretical and experimental point of view.

1.3 Motivation for the work

The polyolefins studied here have precisely controlled molecular structures which make it possible for us to study independently the effects of various molecular characteristics on rheological behavior. In this work the new propylene/ethylene copolymers based on post-metallocene catalysts were studied to explore the reasons for the low viscosity with high filler content both from molecular theory and rheological experiments. This type of study was impossible with traditional polyolefins.

References

1. Shan, C. L. P., *Approaches to Tailoring the Structure and Properties of Polyethylene* , Ph.D Thesis presented to the University of Waterloo, Ontario, Canada, 2002
2. Kim, J. D., *Synthesis of Polyolefins with Controlled Distributionsof Molecular Weight and Chemical Composition by Selective Combination of Supported Metallocene/MAO Catalyst*, Ph.D thesis presented to the University of waterloo, Waterloo, Ontario, Canada, 1999
3. Swogger, K. W., Poon, B., Stephens, C. H., Ansems, P., Chum S., Hiltner, A., and Baer, E., *Material Classification and Applications of New Propylene-Ethylene Copolymer* 1768/ANTEC, 2003
4. Hiltner, A., Dias, P. S, Poon, B., Ronesi, V., Chang, A., Ansems, P., Baer, E., *Elastomeric Properties of New Propylene-Ethylene Copolymers Under Cyclic Loading* 1780/ANTEC, 2003
5. Sexton, D., Ansems, P., Hazlitt, L., *Plastics Innovation from Dow* , Paper presented at 'International Polyolefins 2004', Houston, Texas, 2004

* Trademark of The Dow Chemical Company

Chapter 2. Rheology of Filled Polymeric Systems

Rheology of filled polymer systems is an ever expanding field in polymer industrial research today. How to define a concise, practical and simple format to explain the concepts behind filled polymer systems and the rheological techniques involved in studying their behavior is a big challenge. In this work, the experimental copolymer systems have a unique chain microstructure which produces interesting properties through a broad crystallinity distribution and a unique morphology. Especially, the feature of exceptionally high filler loading provides the potential for reduced material cost and increased sound-deadening capability. A mechanism of the composites is proposed to interpret the exceptionally low viscosity.

Rheological behaviors of multiphase systems are very complicated because of many effects which are specific to the system components. Generally, the properties of filled melts are dominated either by the polymer or by the filler.

In this chapter, the rheological properties of polymers and their filled systems are studied. A summary of some previous work, including the melt-state microphase separation, the concept of interfacial slip and its effect on viscosity, and particle surface treatment, is presented. These concepts are very useful for our understanding on the rheological behavior of our experimental materials.

2.1 Rheological Properties of Polymers

Polymers are classified as viscoelastic materials. The viscoelastic properties of molten polymers are very important for plastics engineers. These properties dominate the processing behavior in the melt state. Therefore, it is critical for plastics engineers to understand the rheological properties of polymers. We also can get some information

about molecular structure of polymers, fillers, and filler-matrix interfacial interaction from rheological properties. This information is an important part of materials characterization.

2.1.1 Linear Viscoelastic Behavior of Polymers

2.1.1.1 Definition of Linear Viscoelasticity[1]

Linear viscoelasticity is the simplest type of viscoelastic behavior. If the strain is small enough, and the molecules of the polymer are disturbed from their equilibrium configuration to a negligible extent, then the relaxation modulus of a polymeric liquid becomes independent of strain (Equation 1), we call this small-strain behavior linear viscoelasticity.

$$\sigma(t) = G(t)\gamma_0 \tag{1}$$

Where $\sigma(t)$ is the shear stress, $G(t)$ is shear stress relaxation modulus and γ_0 is the magnitude of a step in shear strain (at t=0) in a step shear experiment.

Also in the case of linear viscoelasticity, the shear stress and the shear rate have a linear relationship,

$$\sigma(t) = \eta_0\dot{\gamma}(t) \tag{2}$$

η_0 is the zero shear viscosity, and $\dot{\gamma}(t)$ is the shear rate.

Linear viscoelasticity is often used in the comparison of different resins as a method for characterizing the molecules in their equilibrium state.

2.1.1.2 Small amplitude linear oscillatory shear

To determine the linear viscoelastic properties of polymeric liquids, small amplitude linear oscillatory shear is widely used. In this experiment, a shear strain as a sinusoidal function of time is imposed on a sample, $\gamma(t)=\gamma_0\sin(\omega t)$. If γ_0 is sufficiently small the response is linear, and the resulting stress is a sinusoidal function of the same frequency as the strain, $\sigma(t)=\sigma_0\sin(\omega t+\delta)$, where δ is the phase angle which is called the mechanical loss angle.

The stress can be rewritten as:

$$\sigma(t)=\gamma_0\left[G'(\omega)\sin(\omega t)+G''(\omega)\cos(\omega t)\right] \qquad (3)$$

Where $G'(\omega)$, the storage modulus, is a measure of the "degree of elasticity" of the material and $G''(\omega)$, the loss modulus, is a measure of its "degree of viscosity", ω is the frequency.

$G'(\omega)$ and $G''(\omega)$ are calculated from experimental data with the following two equations:

$$G'(\omega)=\frac{\sigma_0}{\gamma_0}\cos(\delta) \qquad (4)$$

$$G''(\omega)=\frac{\sigma_0}{\gamma_0}\sin(\delta) \qquad (5)$$

Sometimes it is convenient to think of $G'(\omega)$ and $G''(\omega)$ as the real and imaginary components of a complex modulus $G^*(\omega)$. Where

$$G^*(\omega)=G'(\omega)+iG''(\omega) \qquad (6)$$

An alternative representation of the results of a small amplitude oscillatory shear test involves η^* (complex viscosity).

Where the complex viscosity η^* is:

$$\eta^*(\omega) \equiv \eta'(\omega) - i\eta''(\omega) \tag{7}$$

and:

$$|\eta^*| = \sqrt{(\eta')^2 + (\eta'')^2} \tag{8}$$

2.1.1.3 Zero Shear Viscosity and Relaxation Spectrum

In oscillatory measurements on polymer melts, the frequency (ω) becomes analogous to shear rate ($\dot{\gamma}$), and $\lim_{\omega \to 0} |\eta^*| = \eta_0$. The zero-shear viscosity (η_0) of polymer melt can be calculated using the $H(\lambda)$:

$$\eta_0 = \int_0^\infty H(\lambda) d\lambda \tag{9}$$

Where $H(\lambda)$ is the relaxation spectrum and λ is the relaxation time.

The shear relaxation modulus, $G(t)$, also can be expressed in terms of $H(\lambda)$:

$$G(t) = \int_0^\infty H(\lambda)\left[\exp(-t/\lambda)\right] d\ln\lambda \tag{10}$$

Where $H(\lambda) d\ln(\lambda)$ is the contribution to the relaxation modulus between $\ln\lambda$ and $\ln\lambda + d\ln\lambda$.

2.1.1.4 Time temperature superposition

Time-temperature superposition (also frequency-temperature superposition or the method of the reduced variables) is a well-known procedure frequently used to either determine the temperature dependence of the rheological behavior of a polymeric liquid

or to expand the time or frequency regime at a given temperature at which the material behavior is studied.

When all linear viscoelastic properties obey the time temperature superposition principle, the equation below is valid for all values of t_r.

$$G_r(t_r) = \sum_{i=1}^{N} G_i(T_0) \exp\left[-t_r / \lambda_i(T_0)\right] \tag{11}$$

Where $t_r \equiv t / a_T$, a_T is the shift factor which can be determined by measuring the temperature dependence of the zero shear viscosity. An empirical relationship for a_T is the Arrhenius equation:

$$a_T = \frac{\eta_0(T)}{\eta_0(T_0)} = \exp\left[\frac{E_a}{R}\left(\frac{1}{T} - \frac{1}{T_0}\right)\right] \tag{12}$$

Where E_a is an activation energy for flow. The equation above is valid as long as the temperature is at least 100K above T_g. Figure 2.1 is a typical example of the time-temperature superposition principle.

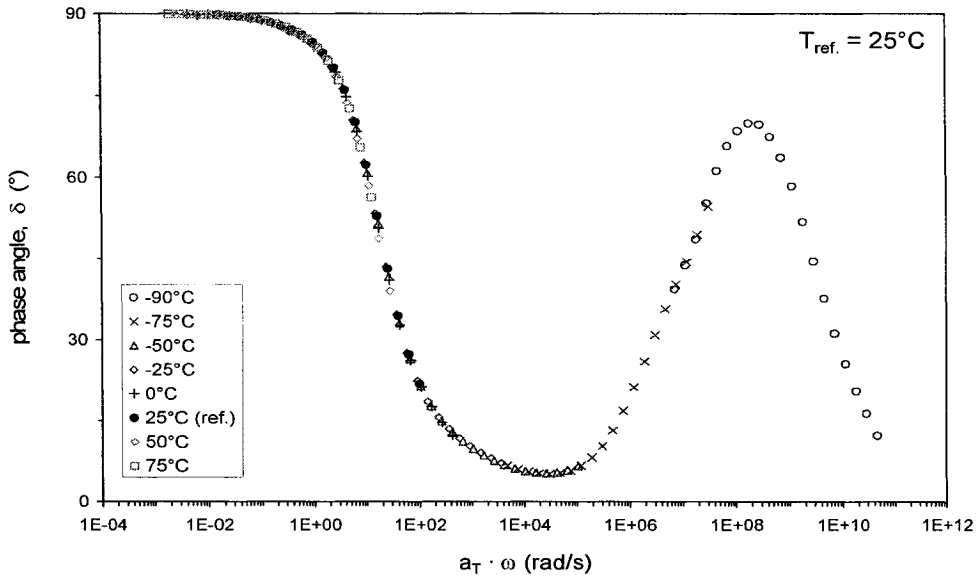

Figure 2.1 Effects of temperature: time-temperature superposition

Time-temperature superposition is a very useful tool for material analysis. But since the different components of a material might display a different temperature-dependency, the time-temperature superposition principle often does not hold for blends [2] and for other systems with relaxation mechanisms that have different temperature sensitivities.

2.1.2 Steady-State Shear Viscosity

Steady-state simple shear flow is very important in applied rheology due to its application in polymer extrusion. Also simple shear viscometric flow is the easiest to generate in the laboratory. Steady parallel disk flow, steady cone and plate flow and steady tube flow are widely used to measure viscosity in the laboratory.

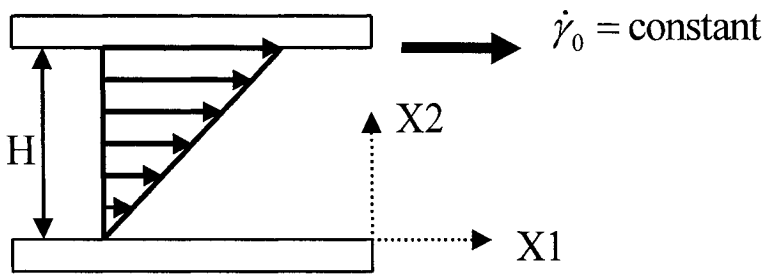

Figure 2.2 Steady simple shear flow

Typically the viscosity of molten polymers is a constant value η_0 at low shear rates, and begins to drop from η_0 as the shear rate increases. At higher shear rates the viscosity exhibits a "power law" behavior. The variation of viscosity with shear rate is dependent upon the molecular weight distribution (MWD).

2.2 Orders in the Melt State

In the melt state, chains of different compositions may self-assemble into various ordered structures.

Propylene-ethylene diblock copolymers have shown an order-disorder transition (ODT) in the melt state due to the microphase separation [3]. Lamellar structure has been detected in the melt state. Dynamic testing results exhibited a limiting behavior of $G' \propto G'' \propto \omega^{0.5}$ in the terminal zone which is an indicator of inhomogeneity.

Polyolefin blends are widely used in many industries, and the most important concern is their miscibility. Since all saturated hydrocarbon polymers have the same formula (CH_2), this chemical structure results in no "specific attractions" due to the lack of polarity and functionality [4]. A typical example is the blend of polyethylene and

polypropylene. Phillip Choi [5] et al proposed a simulation by a molecular dynamics to interpret the possible origin of melt state incompatibility of PP/PE blends. The polypropylene and polyethylene chains were found to segregate into distinct domains. The immiscibility of PP/PE blends may be due to the differences in local morphology in the melt state.

The chemical similarity of the molecular structure for the saturated hydrocarbon polymers makes it more difficult to determine the miscibility than for other polymer blends. To detect the miscibility in the melt, small angle neutron scattering (SANS) is often used providing the direct information about the thermodynamic interactions which govern phase behavior. Recently thermorheological research was introduced to detect inhomogeneity in the melt state. Winesett et al [6] examined the structure formation in symmetric blend films of polystyrene and poly(methyl methacrylate) during phase separation and correlated it to the melt state by time-temperature superposition principle. The principle of time-temperature superposition (TTS) was used to verify qualitatively the temperature-dependent morphology development.

Rheology is a very powerful tool to evaluate the polymer structure and composition. But its disadvantage is that it can not provide a direct measurement of inhomogeneity.

2.3 Rheology of Filled Polymeric Systems

2.3.1 The Einstein Equation [7]

The simplest multiphase system is a dilute suspension of rigid spheres that do not experience Brownian motion in a Newtonian fluid. The shear viscosity $\eta(\phi)$ can then be described simply by the Einstein formula:

$$\eta_r = 1 + 2.5\phi \tag{13}$$

Where η_r is the relative viscosity $\eta_r = \eta(\phi)/\eta_m$, η_m is the medium viscosity, and ϕ is the volume fraction.

2.3.2 Particle-Matrix Interfacial Interactions

Particle-matrix interfacial adhesion greatly affects the rheological behavior of multiphase systems. Usually polymers can form different bonds with selected fillers. These bonds may be due to van der Waals, polar, or hydrogen bonding forces. Also polymers can be covalently bonded to fillers through a coupling agent. To achieve a better dispersion of particles, we usually improve the interfacial interaction. Greater particle-matrix adhesion results in a lower agglomeration of particles. This is not the only approach though. To achieve a better dispersion of particles, two methods are often used. One is to increase the surface energy of particles and improve the interfacial adhesion. The other is to decrease the surface energy of particles and lower the tendency of particle-particle interactions.

2.3.2.1 Surface Tension and the Work of Adhesion

Surface tension is related to surface wetting capability. The best wetting characteristics of particles were reported when the contact angle becomes zero or less than zero [8]. Surface treatment of solid calcium carbonate with the surfactant stearate (Figure 2.3) creates a surface active film between the polymer and the particles. Wetting of the filler allows for improved low energy dispersion. It was reported that surface energy of uncoated calcium carbonate is 200 mJ/m^2 and 40 mJ/m^2 after coating with stearic acid [9-10] (See Figure 2.3). At the liquid-solid interface, if the molecules of the liquid have a stronger attraction to the molecules of the solid surface than to each other (the adhesive forces are stronger than the cohesive forces), then wetting of the surface

occurs. Alternately, if the liquid molecules are more strongly attracted to each other and not the molecules of the solid surface (the cohesive forces are stronger than the adhesive forces), then the liquid beads-up and does not wet the solid surface.

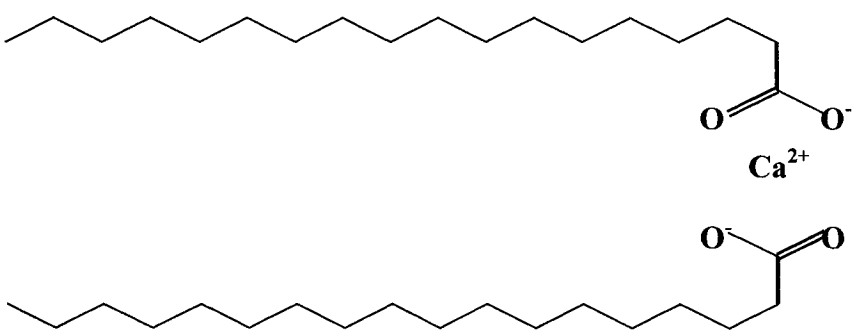

Figure 2.3 Calcium stearate ($C_{36}H_{70}CaO_4$)

A particle surface coating can also cause the viscosity of the filled melt to decrease significantly by promoting slip between the particles and the matrix. The interface is the heart of the composite because of its role in transferring stresses between the matrix and the filler. Surface treatment of calcium carbonate with stearate will cause a gradual lowering of adhesion between the phases due to a significant lowering of interactions. Usually contact angle measurements are used to evaluate particle-matrix adhesion.

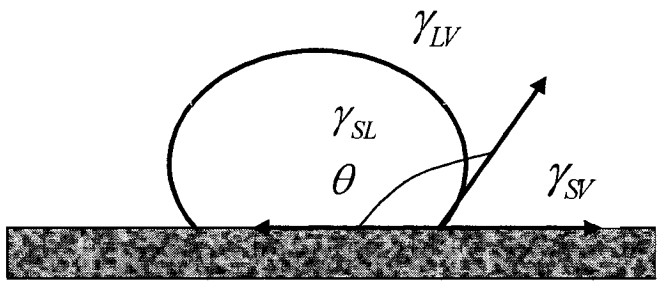

Figure2.4 A polymer droplet on a substrate at equilibrium

The equilibrium contact angle for a liquid drop on smooth, homogeneous, and rigid surface is related to the various interfacial tensions by the Young equation: [11]

$$\gamma_{LV}\cos\theta = \gamma_{SV} - \gamma_{SL} \tag{14}$$

Where γ_{LV} is the surface tension of the liquid in equilibrium with its saturated vapor, γ_{SV} is the surface tension of the solid in equilibrium with its saturated vapor, and γ_{SL} is the interfacial tension between the solid and the liquid. The work of adhension is as follows:

$$W_{adh} = \gamma_{SV} + \gamma_{LV} - \gamma_{SL} \tag{15}$$

So we can get:

$$W_{adh} = \gamma_{LV}(1+\cos\theta) \tag{16}$$

Therefore, we can calculate the work of adhesion directly based on the two quantities γ_{LV} and θ that can be extracted from the same experiment. In the equation above, γ_{LV} can be calculated by the sessile drop analysis through the Bashforth-Adams set of equations.

2.3.2.2 Concept of Ideal Slip [12]

The slip between a melt and a solid can be quantitatively specified in terms of the extrapolation length $b = \eta_m / \beta$, where η_m is the medium viscosity and β is the friction coefficient. The extrapolation length is defined in Figure 2.5.

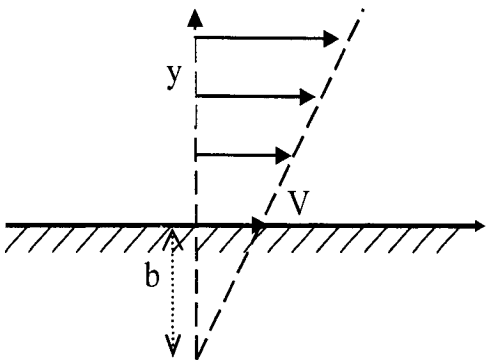

Figure 2.5 An idealized view of shear flow near a surface

We can make b as large as possible in two steps: (a) achieve the weakest interfacial interaction between the solid $CaCO_3$ particles and P/E copolymer melt by lowering the surface energy, and (b) use P/E copolymers with the highest viscosity η_m. Generally, interfacial slip may have significant effects only when b is large relative to the particle size.

In reality, polymer chains are often attached fairly strongly on the solid surface, making it very difficult to achieve interfacial slip under relatively low stresses. However, at weak interfaces, the polymer molecular weight and temperature greatly affect the interfacial interactions which may result in solid-matrix interfacial slip. Chain desorption will occur at a lower onset stress σ_c for a suspension of higher molecular weight. The onset stress for the interfacial slip is significantly higher at a lower temperature. This

suggests that it is the stress-induced chain desorption causing the interfacial slip at the weak interfaces and is not the chain disentanglement transition.

Based on Eyring's theory[11] for the viscosity of liquids, an equation for the critical shear stress for the onset of slip, σ_c, as a function of the work of adhesion, is

$$\sigma_c = \frac{2fW_{adh}}{d} \tag{17}$$

Where f is the fraction of interfacial adhesion, d is the jumps of polymer chain which is smaller than but comparable to its radius of gyration.

2.3.2.3 Slip Transition

At weak interfaces, a transition will take place between a regime of weak slip at low slip velocity and a regime of strong slip at high slip velocity. In the weak-slip regime, b is almost constant, and for very large slip velocities, b has a tendency to saturate, as shown in Figure 2.6.

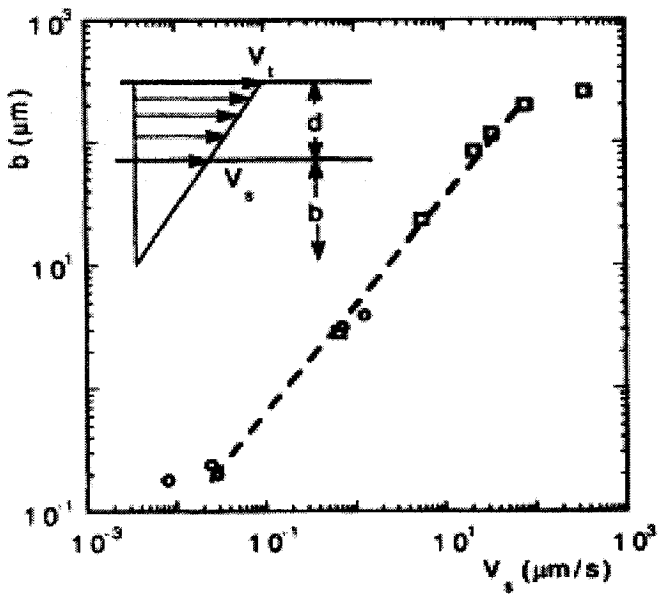

Figure 2.6 Slip transition [13]

If long polymer chains are grafted on a solid interface (strong interface), the slip is greatly reduced, but does not disappear [14]. In this case, one has a transition from stick to slip boundary condition. Migler and Leger et al [13, 15-16] and Drda and Wang et al [17] proposed the mechanism of stick-slip transition. Meanwhile, some direct measurements on local velocity of polymer melt have been published. The measurements show that the sharp transition will occur on weak solid-polymer melt interfaces under high shear stress and the onset stress agrees well with the stick-slip mechanism. As to the strong interface, moderate transition can be observed. Also F. Brochard et al [18] indicated that slip which occurs at the melt-particle and melt-wall interface will result in reduced apparent viscosity.

2.3.3 The Modified Einstein Formula [12]

In the case of interfacial slip, the modified Einstein formula applies:

$$\eta_{(\phi)} = \eta_m \left[1 + \frac{5(1+2b/R)}{2(1+5b/R)} \phi \right] \tag{18}$$

Where R is the sphere radius, η_m is the medium viscosity, b is the extrapolation length characterizing the sphere-medium interfacial interactions, and $\eta_r = \eta_{(\phi)} / \eta_m$ is the relative viscosity.

2.4 Surface Treatment of Calcium Carbonate Particulates

Calcium carbonate is the particulate filler most widely incorporated into polymers both to modify the solid-state state properties and to reduce cost. The properties of resulting composites are dependent upon the filler content, its size and shape (distribution), its dispersion and the particle-matrix interface. Usually before incorporation into plastics, calcium carbonate is surface treated in order to achieve a better dispersion and also to

improve the solid-state properties. The most widely used calcium carbonate coating is stearic acid. [19] In this case, a very thin organic film is attached on the particle surface which has a strong influence on the properties of the composites. US patent 6569527 [20] described a detailed method for coating calcium carbonate. Further research [19] indicated that the resulting organic film is a monolayer of hydrophobic molecules which has a thickness of 2.6 nm corresponding to the molecular length of stearic acid. The use of excess stearic acid leads to the formation of a bilayer as well as to free acid molecules. Also, the excess coating amplifies the reinforcing effect on the stiffness but reduces all other mechanical properties of the composites. [21] Rheological results [22] indicated that the organic monolayer on the particle surface lubricated the polymer flow and led to an additional shear thinning at high shear rate.

In a polymer matrix, it is necessary to have a good wetting on the particle surface. However, the adhesion between particle and matrix should not be too strong, because particle-matrix interfacial debonding imparts toughness to the composites [23-25].

References

1. Dealy, J. M., Wissbrun, K. F., *Melt Rheology and its Role in Plastics Processing:Theory and Applications* ,Published by Kluwer Academic Publishers, Reprinted in 1999
2. D'Orazio, L., Mancarella, C., Martuscelli, E., Sticotti, G., and Cecchin, G., I*sotactic Polypropylene /Ethylene-co-Propylene Blends: Influence of the Copolymer Microstructure on Rheology, Morphology, and Properties of Injection-Molded Samples*, Journal of Applied polymer Science, Vol.72, 701-719, 1999
3. Sakurai, K., MacKnight, W. J., Lohse, D. J., Schulz, D. N., Sissano, J. A., Wedler, W., and Winter, H. H., *Dynamic viscoelastic properties of poly(ethylene-propylene) diblock copolymer in the melt state and solutions*, Polymer Vol. 37 No. 23, 5159-5163, 1996
4. Lohse, D. J., and Garner, R. T., Graessley W. W., and Krishnamoorti R., *Miscibility of blends of saturated hydrocarbon elastomers* Rubber Chemistry and Technology; Vol 72, 4, 569-573, Sep/Oct 1999
5. Choi P., Blom, H. P., Kavassalis, T. A. and Rudin A., *Immiscibility of polyethylene and polypropylene: A molecular dynamics study*, Macromolecules, Vol.28, 8247-8250, 1995
6. Winesett, D. A., Zhu, S., Sokolov, J., Rafailovich, M., and Ade, H., *Time–temperature superposition of phase separating polymer blend films*, High Performance Polymers, Vol 12, 599–602, 2000
7. Carreau, P. J., Kee, D. C. R. D., Chhabra, R. P., *Rheology of Polymeric Systems: Principles and Applications*, Hanser/Gardner Publications Inc. 1997

8. Akovali, G., *The Interfacial Interactions in Polymeric Composites*, Kluwer Academic Publishers, Dordrecht, June 1992

9. Omya International AG, *Physicochemical Aspects of Minerals components for Plastics Processors,* Switzerland, 2002

10. Pukanszky. B., Karger-Kocsis J., *Polypropylene: structure, blends and composites.* London: Chapman and Hall; 1995. Chapter 1

11. Anastasiadis S. H., and Hatzikiriakos, S. G., *The Work of Adhesion of Polymer/Wall interfaces and its association with the onset of wall slip* Journal of Rheology .42(4), July/August 1998

12. Inn, Y. W., and Wang, S. Q., *Molecular Interfacial Slip between Solid and Liquid in Polymer Suspensions of Hard Spheres*, Langmuir 11,1589-1594,1995

13. Migler, K. B., Massey, G., Hervet H., and Leger, L., *The slip transition at the polymer-solid interface, Journal of Physics:Condense Matter*, Vol.6 A301-A304, 1994

14. Dubbeldam J. L. A., and Molenaar, J., *Self-consistent dynamics of wall slip*, Physical Review E, Vol.67, 011803, 2003

15. Migler, K. B., Hervet, H., and Leger, L., *Slip Transition of a Polymer Melt under Shear Stress*, Physical Review Letters, Vol.70, 3, 1993

16. Leger, L., Hervet, H., Massey, G., and Durliat, E., *Wall Slip in Polymer Melts*, Journal of Physics: Condensed Matter, Vol.9, 7719-7749, 1997

17. Drda, P. P., and Wang, S. Q., *Stick-Slip Transition at Polymer Melt/Solid Interfaces*, Physical Review Letters, Vol. 75, 14, 1995

18. Brochard, F., and Gennes, P.G., *Shear Dependent Slippage at a Polymer/Solid Interface*, Langmuir 8, 3033-3037, 1992

19. Osman, M. A., and Suter, U. W., Surface *Treatment of Calcite with Fatty Acids: Structure and Properties of the Organic Monolayer*, Chemical matters, 14, 4408-4415, 2002

20. Calhoun, A. A., Shurling, D. S., Skelhorn, D. A., and Ansari, D. M., *Particulate Carbonates and Their Preparation and Use in Thermoplastic Film Compositions*, US 6569527, May 27, 2003

21. Osman, M. A., Atallah, A., and Suter, U. W., *Influence of Excessive Filler Coating on the Tensile Properties of LDPE–Calcium Carbonate Composites*, Polymer 45, 1177-1183, 2004

22. Osman, M. A., Atallah, A., Schweizer, T., and Öttinger, H. C., *Particle–Particle and Particle-Matrix Interactions in Calcite Filled High-Density Polyethylene-Steady Shear*, Journal of Rheology, 48(5), 1167-1184, 2004

23. Price, G. J., and Ansari, D. M., *Surface Modification of Calcium Carbonates Studied by Inverse Gas Chromatography and the Effect on Mechanical Properties of Filled Polypropylene*, Polymer International, 53:430-438, 2004

24. Zuiderduin, W. C. J., Westzaan, C., Huétink, J., Gaymans, R. J., *Toughening of Polypropylene with Calcium Carbonate Particles*, Polymer 44:261-275, 2003

25. Wang Y., and Lee, W. C., *Interfacial International in Calcium Carbonate-Polypropylene Composites. 2: Effect of Compounding on the Dispersion and the Impact Properties of Surface-Modified Composites*, Polymer Composites, Vol.10, No.5, October 2004

Chapter 3. Objectives of Research

The primary objective of this project is to produce a fundamental understanding of the lower viscosity of the novel P/E copolymers highly filled with particulates. Our goal is to thoroughly characterize the rheological behavior of $CaCO_3$ filled new P/E copolymers.

The secondary objective is to provide new knowledge about the rheological behavior of particulate filled polymer melts in shear flow and to relate this aspect of the behavior to the structure of the polymer, particle surface treatment, and composite microstructure.

Chapter4. Experimental Studies

The experimental studies include four major parts:

- Experimental materials
- Thermorheological behaviors of pure resins
- Small amplitude oscillatory shear tests
- Steady-state shear viscosity measurements

In this chapter, different methods for viscosity measurements and linear viscoelasticity tests are described. Specific experimental techniques like step-shear rate for measuring the steady shear viscosities, oscillatory time sweep for monitoring the microstructure evolution and rough plates for minimizing the bulk slip are described.

4.1 Experimental Materials

4.1.1 Matrix Materials

The copolymer of primary interest (N-P/E) is a new resin produced by The Dow Chemical Company. It is a linear, isotactic propylene-ethylene copolymer based on Dow's post-metallocene catalyst technology. This copolymer has a broad chemical composition distribution and narrow molecular weight distribution.

For comparison purposes a conventional metallocene-based propylene-ethylene copolymer (m-P/E) and a constrained geometry catalyst technology (CGCT) based ethylene-octene copolymer (E/O) are also included. The m-P/E has a narrow molecular weight distribution and narrow chemical composition distribution as does the E/O copolymer. All materials were provided by The Dow Chemical Company.

Table 4.1 Matrix materials

Materials	Mw g/mol	Mw/Mn	MFR g/10min	Ethylene Content wt%	Melting Behavior °C
N-P/E	141500	2.85	25 *	12	52-132
m-P/E	157800	2.1	25 *	7.7	105
E/O	79900	2.07	5 +	62	63

*ASTM D-1238 T=230°C, 2.16kg, + ASTM D-1238 T=190°C, 2.16kg

All pure resin samples for rheometry were prepared by compression molding on a Caver Laboratory Press (Model 2114), following the detailed preparation method of Kang Zhu [1]. All the samples were molded at temperature of about 150°C.

Filled samples were blended with filler and hot-pressed by technicians at The Dow Chemical Company. The sample disks for rheometry (thickness of 1.2-1.5 mm, diameter of 25mm) were cut from the molded sheets.

4.1.2 Filler Calcium Carbonate

The filler particles, FILMLINK 400, are a product of IMERYS® Minerals Ltd. The calcium carbonate particles are made from marble calcite and have a rhombohedral shape with an aspect ratio of 3 and an average diameter of 1.2-1.3 μm. The specific surface area is 8.3565 m^2/g. An SEM image of a typical particle is shown in Figure 4.1.

Figure 4.1 SEM image of a typical particle

Particle analysis was conducted on a Malvern® MasterSizer® LASER diffractor by Particle Technology Labs Ltd. This instrument is considered as an ensemble analyzer that calculates a volume distribution from the LASER (light amplification by stimulated emission of radiation) diffraction pattern of a cloud of particles. The raw scatter data is then processed using a complex algorithm and presented on the basis of equivalent spherical diameter. From Figure 4.2 we find that the filler particles have a very broad particle size distribution.

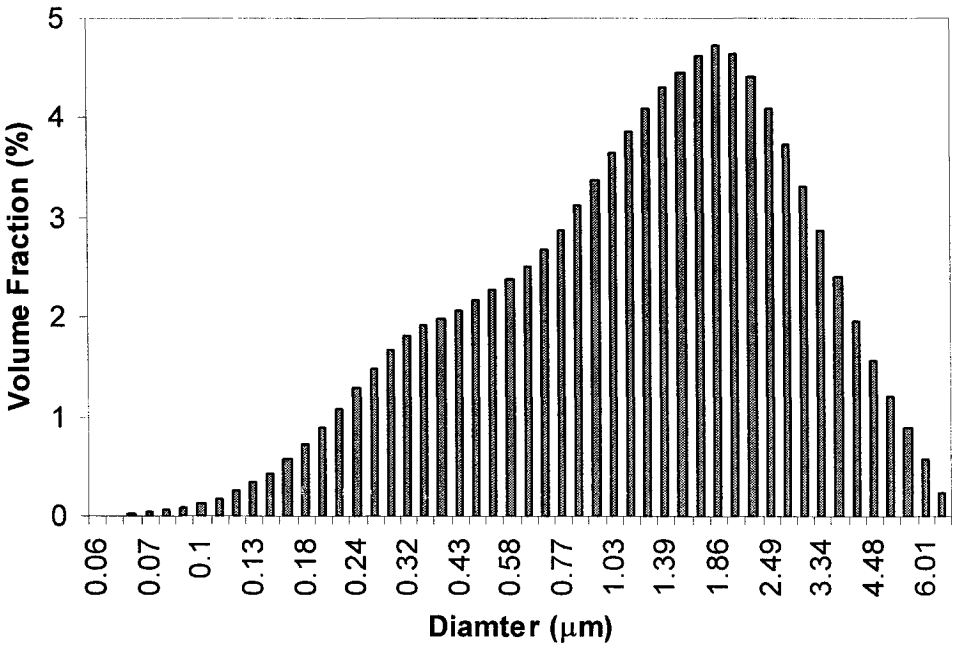

Figure 4.2 Particle size distributions

According to the information supplied by IMERYS, the particles are chemically coated with approximately a monolayer of stearate (approximately 25Å^2 per stearate molecule) via a heated air-swept process. The stearic acid reaction on the particle surface results in the chemisorbed stearate bonded to specific Ca-O bonds with a 1:1 reaction between the Ca^{2+} site and stearate. The stearate molecule is slightly tilted from perpendicular. The chemically bound monolayer is not totally compact.

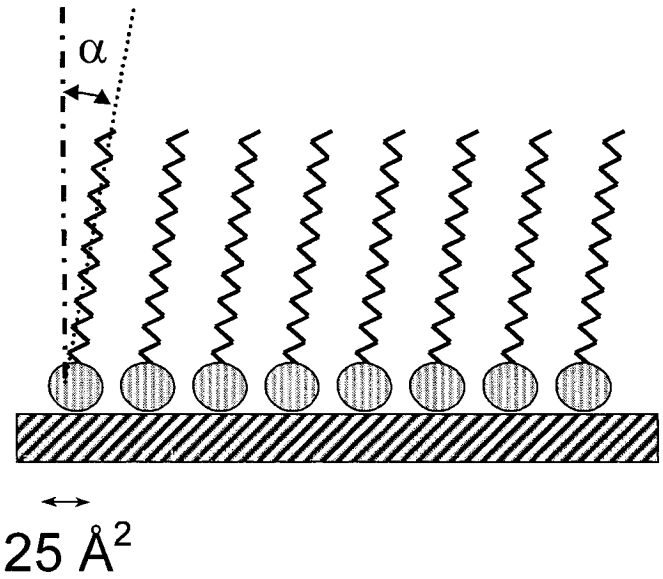

Figure 4.3 Schematic of monolayer of stearate (supplied by IMERYS®)

4.2 Oscillatory Shear Tests

Linear viscoelasticity is the simplest viscoelastic behaviour. LVE behaviour occurs at low deformation rates and small strains. LVE is important due to its high dependency upon molecular structure and material microstructure.

4.2.1 Matrix Resins

All oscillatory shear tests were conducted on an Anton-Paar Physica MCR-500 stress-controlled rheometer with 25mm plate-plate geometry under a nitrogen atmosphere.

Before the oscillatory shear measurements, strain sweep tests and thermal stability tests were performed to determine the testing conditions. The principles of setting testing conditions are as follows:

- Small enough deformation (strain) to ensure the measurements are in the linear viscoelastic (LVE) region throughout the tests
- Thermal stability while the samples are being tested.

- The torques should be in the test range of the MCR-500

To determine the linear viscoelastic range of samples, dynamic strain or stress sweeps are performed. Figure 4.4 shows the results of a strain sweep test of N-P/E at an angular frequency of 100 rad/s and temperature of 160°C. In the region of strain of 0-13%, the complex viscosity is constant and at higher strains it decreases sharply with strain. This means that the LVE region of N-P/E at a frequency of 100 rad/s is 0-13%.

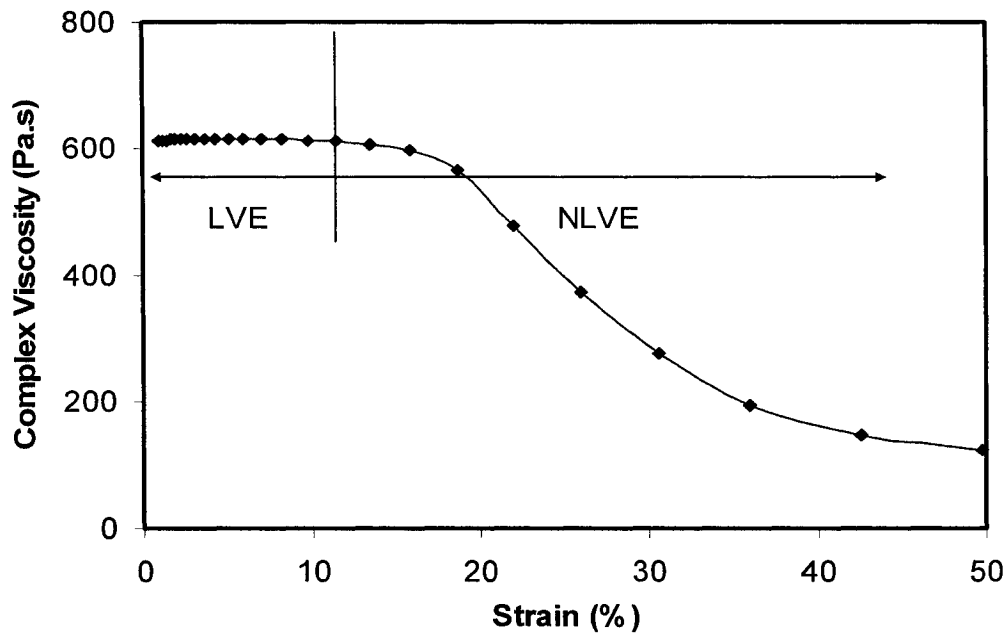

Figure 4.4 The strain sweep of N-P/E at frequency of 100 rad/s and T=160°C

The time sweep test is used to determine the thermal stability of experimental materials at test temperatures. Figure 4.5 shows the results of a time sweep test of m-P/E at a temperature of 160°C.

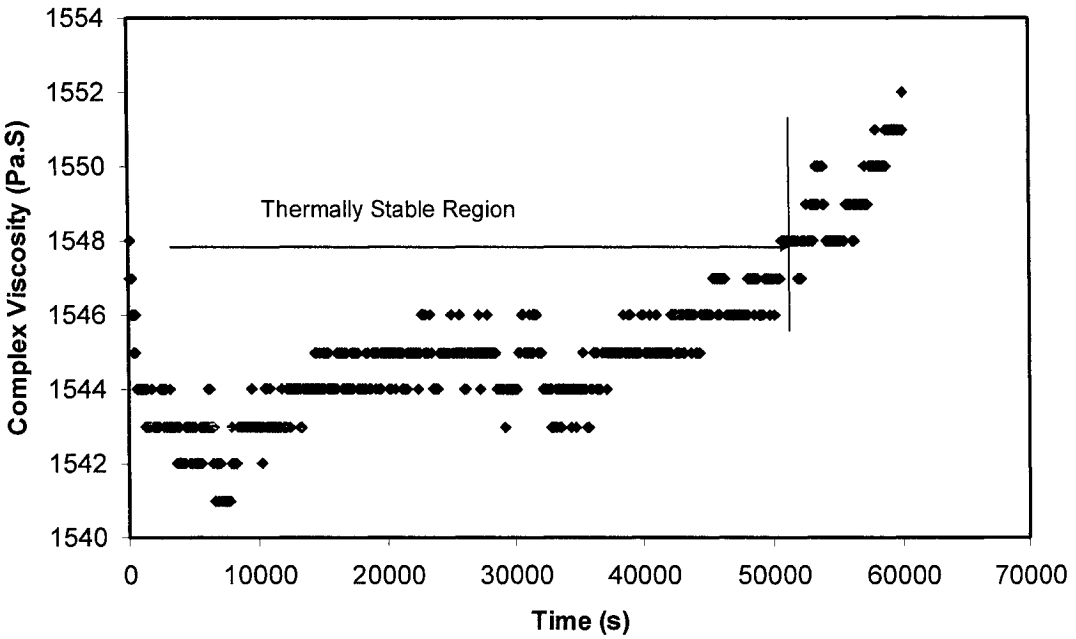

Figure 4.5 The time sweep of m-P/E at frequency of 1 rad/s and temperature of 160°C

The final conditions are listed in Table 4.2. All the measurements were repeated with at least 3 samples at every temperature. Due to the testing noise, some experimental data of storage modulus at low frequency have been truncated. The error bars for standard deviation have been set up on the results for the storage modulus and loss modulus.

Table 4.2 Test conditions for oscillatory shear

Sample	N-P/E		m-P/E		O/E	
Frequency, rad/s	500-1	1-0.01	500-1	1-0.01	500-1	1-0.01
Temperature, °C	160, 180, 200		140, 160, 180		160	
Strain, %	5-7	50	57	50	4	30
Gap, mm	0.5		0.5		0.8	

4.2.2 Filled Samples

All of the filled systems exhibited complicated time-dependent rheological behaviors which made it very difficult to measure the linear viscoelasticity. Since our filled samples were prepared by hot-pressing, particle orientation and agglomeration were inevitably induced in the preparation process. When they were loaded in the rheometer and heated, relaxation of the structure occurs. Due to this relaxation, all of the samples exhibited time-dependent behaviors. To achieve steady and reproducible rheological testing results, every sample was exposed to oscillatory shear in the linear region for a period of time until the complex viscosity reached a constant value. At that point we assume that the relaxation of the orientation is complete and the frequency sweep is then performed. Figure 4.6 and Figure 4.7 show the time sweeps of N-P/E 40% $CaCO_3$ and N-P/E 60% $CaCO_3$ at a frequency of 1 rad/s. Strain sweeps were performed to detect the linear region and to confirm the linear condition of time sweep (Figure 4.8). Table 4.3 and 4.4 are the final testing conditions for the filled systems.

All the dynamic tests for filled m-P/E samples were repeated two times with different samples. Due to the limited time, all the filled N-P/E samples were only repeated once.

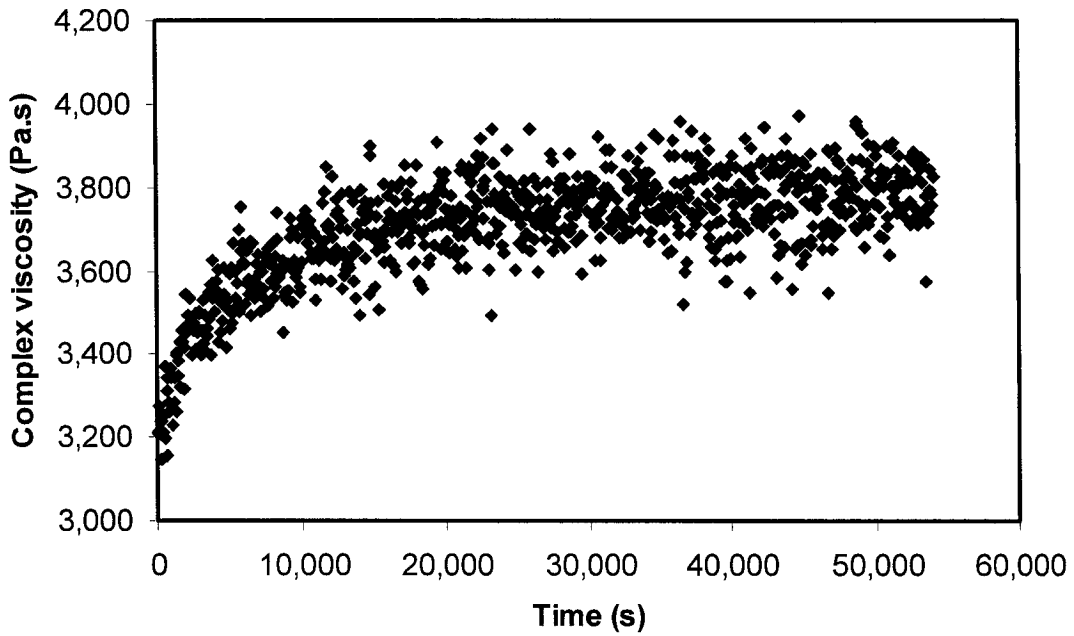

Figure 4.6 Time sweep of N-P/E 40% $CaCO_3$ at γ=0.005%, frequency=1rad/s, T=160°C

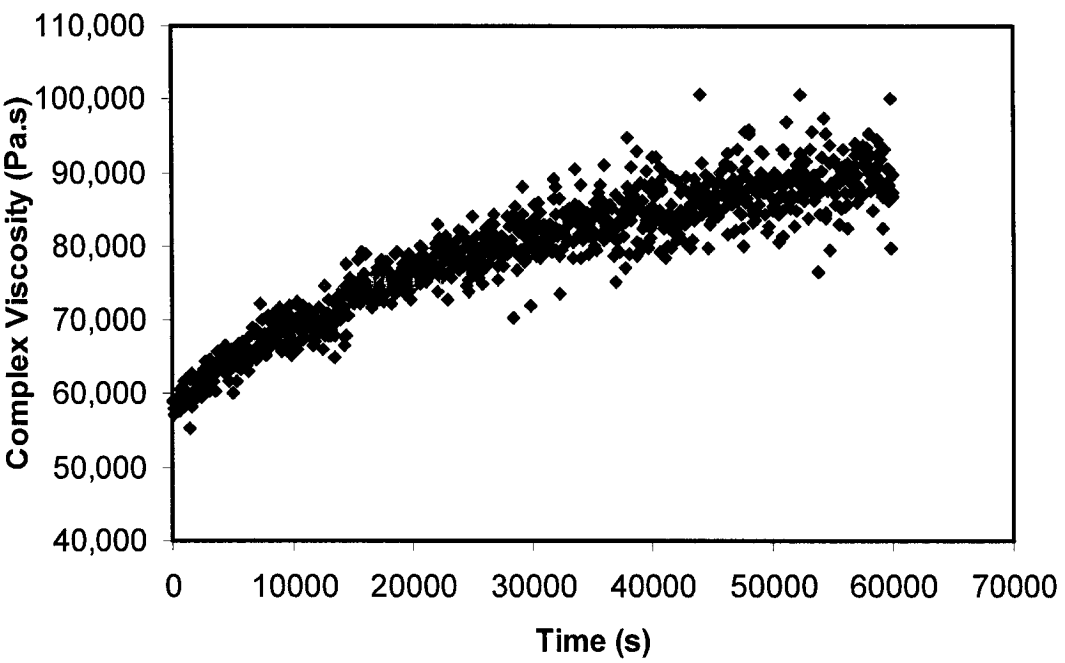

Figure 4.7 Time sweep of N-P/E 60% $CaCO_3$ at γ=0.001%, frequency=1rad/s, T=160°C

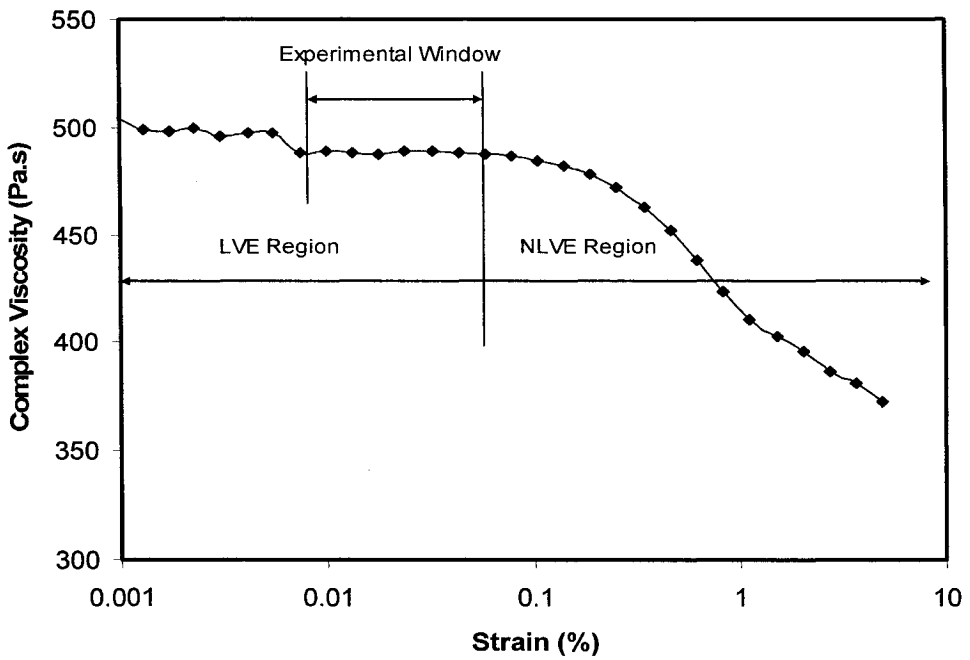

Figure 4.8 The strain sweep of N-P/E 40% $CaCO_3$ at frequency=500 rad/s, T=160°C

Table 4.3 Test conditions of oscillatory shear (filled N-P/E)

Sample	N-P/E 20% $CaCO_3$		N-P/E 40% $CaCO_3$		N-P/E 60% $CaCO_3$	
Frequency, rad/s	500-1	1-0.01	500-1	1-0.01	500-1	1-0.01
Temperature, °C	160		160		160	
Strain, %	0.1	0.1	0.08	0.08	0.01	0.01
Gap, mm	1		1-1.2		1-1.2	

Table 4.4 Test conditions of oscillatory shear (filled m-P/E)

Sample	m-P/E 20% $CaCO_3$		m-P/E 40% $CaCO_3$		m-P/E 60% $CaCO_3$	
Frequency, rad/s	500-1	1-0.01	500-1	1-0.01	500-1	1-0.01
Temperature, °C	160		160		160	
Strain, %	0.1	0.1	0.08	0.08	0.01	0.01
Gap, mm	1		1-1.2		1-1.2	

4.3 Steady-State Shear Test

4.3.1 Cone and Plate Geometry

The cone-plate geometry is the best for shear viscosity measurements. The main advantages [1] are:

- Constant shear rate and no requirement of flow kinematics assumptions

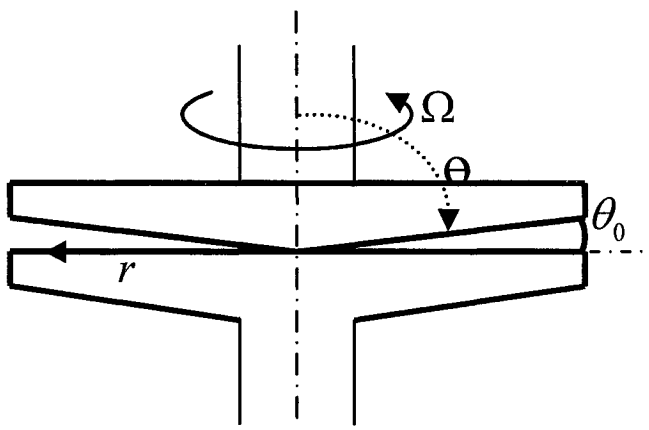

Figure 4.9 A typical cone-plate system

For cone-plate geometry with a very small cone angle, the velocity profile is as follows:

$$\frac{V_\theta}{r} = \Omega \left[\frac{\left(\frac{\pi}{2}\right) - \theta}{\theta_0} \right] \tag{18}$$

Where r is the radial position, θ_0 is the cone angle, and Ω is the angular rotational speed of the cone.

The shear rate is expressed by

$$\dot{\gamma} = \dot{\gamma}_{\theta\phi} = \frac{\sin\theta}{r} \left[\frac{\partial}{\partial\theta} \left(\frac{V_\phi}{\sin\theta} \right) \right] \approx -\frac{\Omega}{\theta_0} \tag{19}$$

Since $\sin\theta \approx 1$ .Therefore, the shear rate is constant.

- Very small samples
- Negligible end effects

Figure 4.9 shows a typical cone-plate system. This is excellent for uniform fluids but can not accommodate fluids which contain particles, because the particles will cause interference where the gap becomes very small at the apex of the cone. Most cones are truncated for easy gap setting, but the truncation is restricted to a very small central portion.

The viscosities of the N-P/E, m-P/E and E/O pure resins were measured by cone and plate rheometry.

4.3.2 Plate-Plate Measuring System

Plate-plate geometry (Figure 4.10) is frequently used to measure the steady shear properties of multiphase systems. The main advantages:

- Easy gap-setting

- Good for multiphase systems
- Negligible capillary effects

Since the flow is not homogeneous within the gap, the shear rate varies with the radial position and the viscosity is not proportional to the torque. In commercial rheometers, the viscosity is calculated from a single torque value, assuming Newtonian behavior which is not appropriate. So a Rabinowitsch-type procedure should be performed to calculate the viscosity from measurements in this geometry. In this work, all the viscosity results for the filled systems were measured and corrected by plate-plate rheometry.

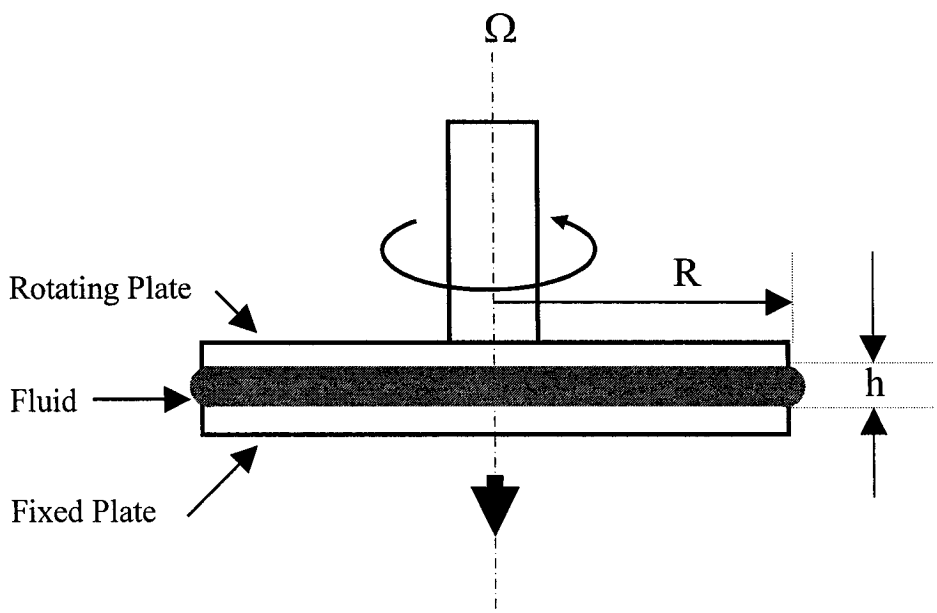

Figure 4.10 Plate-plate measuring system

4.3.3. Viscosity Correction

The detailed method of viscosity correction is described as follows:

The final expression for the viscosity [1] is:

$$\eta_{(\dot{\gamma}_R)} = \frac{T}{2\pi R^3 \dot{\gamma}_R}\left[3 + \frac{d\ln(\frac{T}{2\pi R^3})}{d\ln\dot{\gamma}_R}\right] \tag{20}$$

Where the correction factor is $$n = \frac{d\ln\left(\frac{T}{2\pi R^3}\right)}{d\ln\dot{\gamma}_R} \tag{21}$$

$\dot{\gamma}_R$ is the wall shear rate, T is the torque, and R is the radius of plate.

To use these expressions we:

- Plot *Ln*(torque) vs. *Ln*(shear rate)
- Since then, $n = d(Ln(T))/d(Ln(\dot{\gamma}_R))$
- Fit a curve for $n(\dot{\gamma}_R)$ which will be used to calculate the real viscosity
- For Newtonian fluids, n=1 and no correction is needed

Figure 4.11 shows an example of the viscosity correction factor.

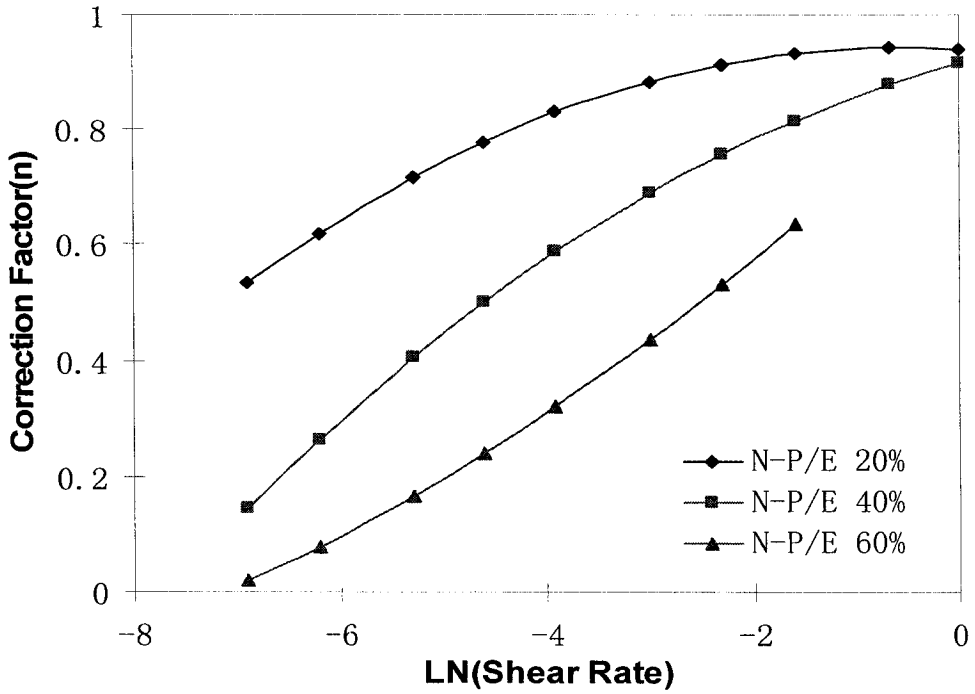

Figure 4.11 An example of viscosity correction

4.3.4 The Cox-Merz Rule

The Cox-Merz rule $\eta(\dot{\gamma}) = |\eta^*(\omega)|, (\omega = \dot{\gamma})$ is a very useful empirical relationship. For most polymers with flexible molecules, the Cox-Merz rule works well. We can determine the complex viscosity over a wide range of frequency and extract the steady-shear viscosity from the complex viscosity in that case.

Figure 4.12 shows the shear viscosity and complex viscosity of the E/O copolymer at 160°C. It is found that the Cox-Merz rule works very well for our E/O copolymer and also for the N-P/E and the m-P/E. Figure 4.13 shows the shear viscosity and complex viscosity of the N-P/E 40% $CaCO_3$ at temperature of 160°C. The Cox-Merz rule does not work for the filled samples due to the different microstructures of filled samples under different flow kinematics.

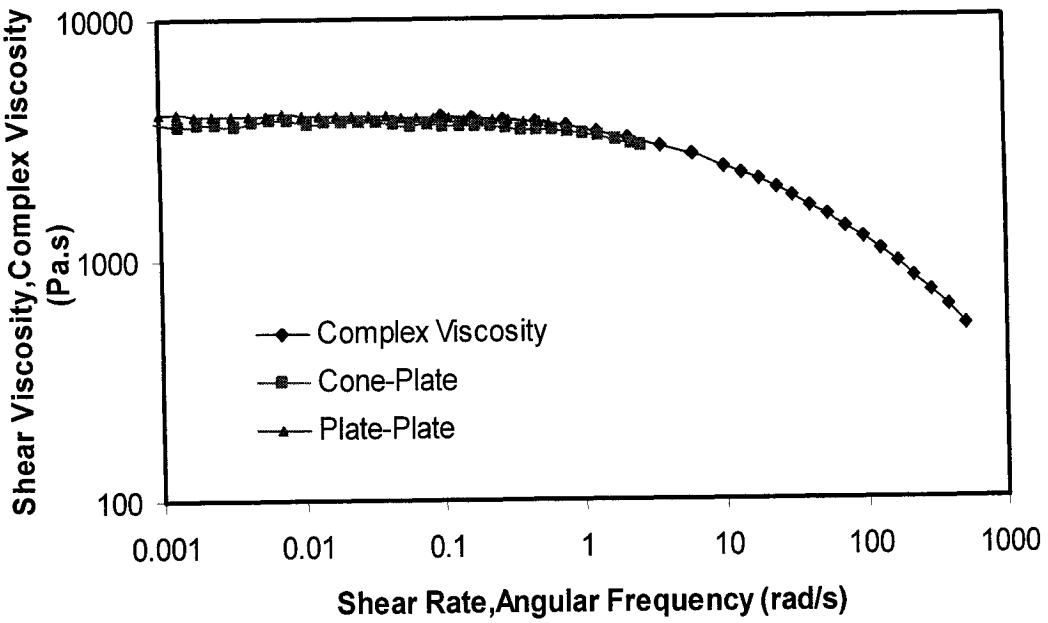

Figure 4.12 The Cox-Merz rule (pure E/O resin at 160°C)

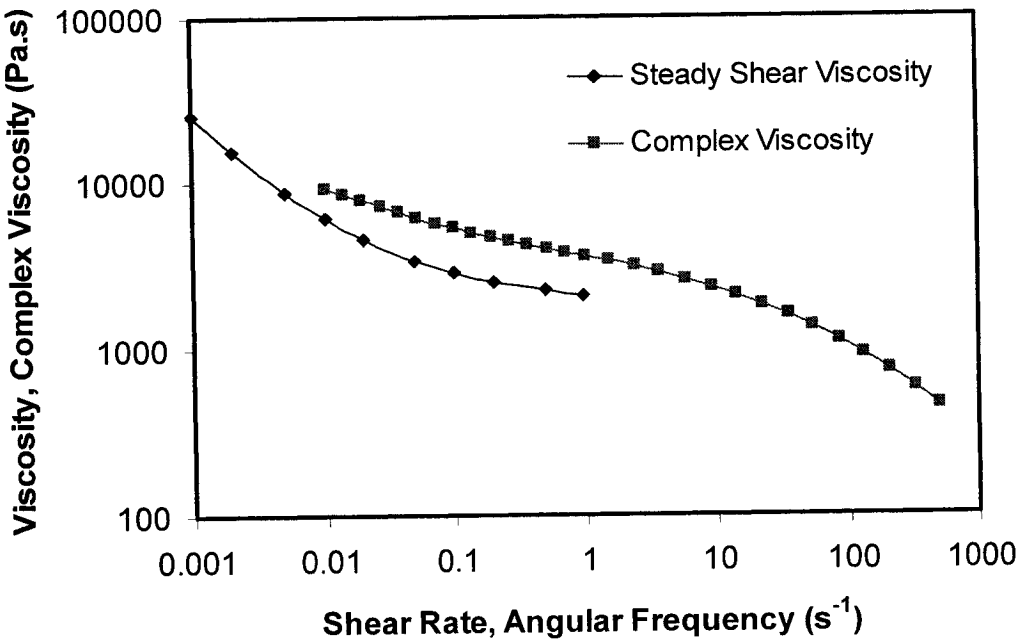

Figure 4.13 The shear viscosity and complex viscosity of N-P/E 40% $CaCO_3$ at temperature of 160°C

4.3.5 Bulk Slip

The biggest problem in the viscosity measurements with the filled samples is bulk slip. To prevent or minimize the bulk slip during the viscosity measurements, a rough plate-plate measuring system was designed. We hoped to measure the viscosities of samples with 80% loading using this system. Figure 4.14 is the schematic of the grooved plates. However, due to the bulk slip, the viscosities of samples with 80% loading can not be measured by regular rotational viscometry even with rough plates. Figure 4.15 shows the bulk slip of N-P/E 80% $CaCO_3$ in shear. Before shearing, the sample is marked by a black marker. After shearing for a period of time, bulk slip was detected from the black mark. For the samples with lower loadings (0-60%), no bulk slip was detected and the non-slip boundary condition applied. Figure 4.16 shows the expected result in the absence of slip.

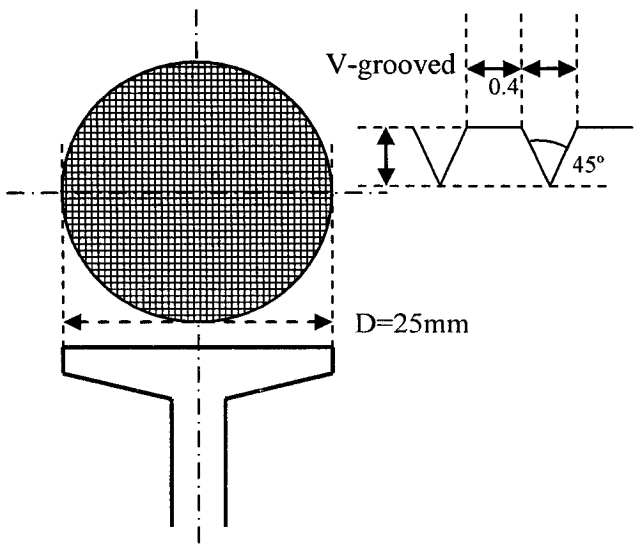

Figure 4.14 Schematic of the grooved plates

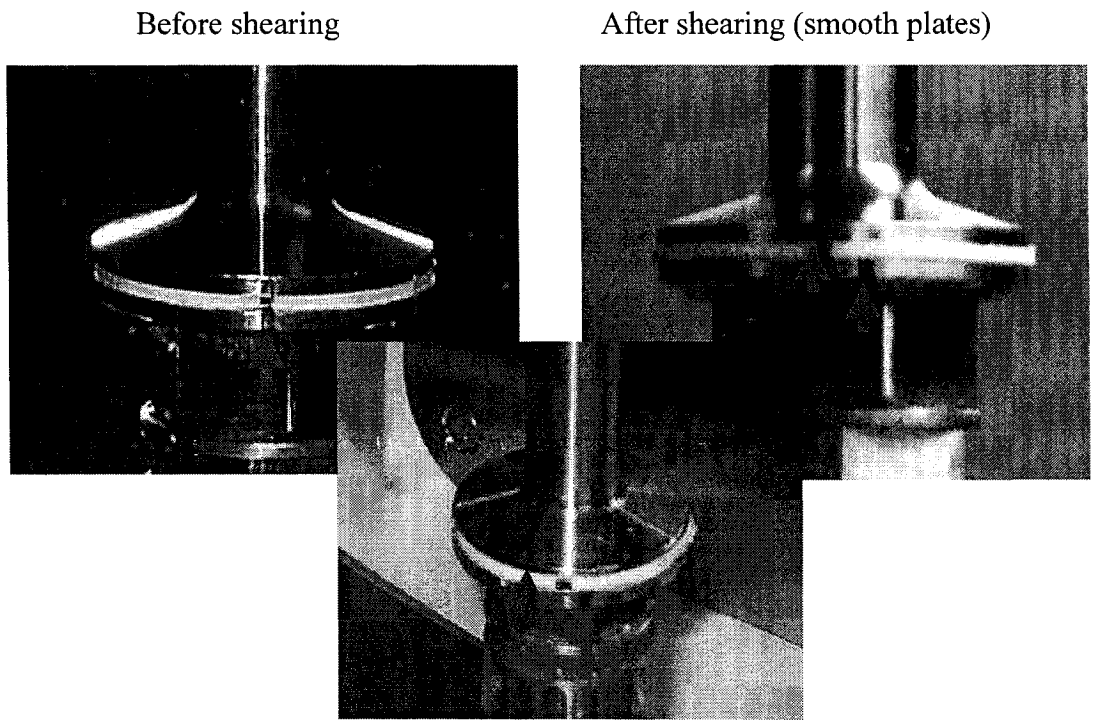

Figure 4.15 Bulk slips (N-P/E 80% $CaCO_3$)

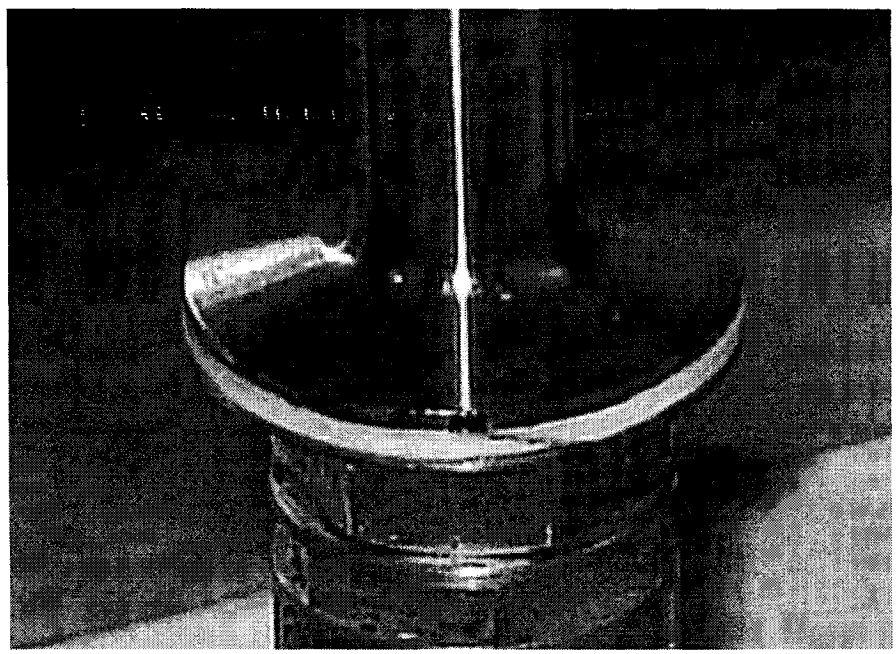

Figure 4.16 Slip-free shear (N-P/E 60% $CaCO_3$)

4.3.6 Time-dependent Viscosity

Rheopexy is a non-Newtonian phenomenon which is related to the complex microstructure and the effects of shear history on the structure of filled systems. In this case, viscosity increases with time at a constant shear rate due to a buildup of structure. Rheopexy is a very complicated phenomenon and the mechanism involved is still not clear.

All of our filled polymer systems exhibit rheopexy. Viscosity increases with time at a constant shear rate for a very long time until steady state is eventually reached. Figure 4.17 is a time sweep of the viscosity of N-P/E 40% $CaCO_3$ at constant shear rate of $0.001s^{-1}$. The steady-state viscosity is reached after 2-hours of shearing. The averaged plateau value is taken as the true viscosity. All filled systems exhibited similar behavior; we attribute this increasing viscosity to shear induced particle-particle interaction. Another example is shown in Figure 4.18. Figure 4.19 shows the stress growth coefficient of N-P/E. The steady-state viscosity is reached very quickly for the pure polymers.

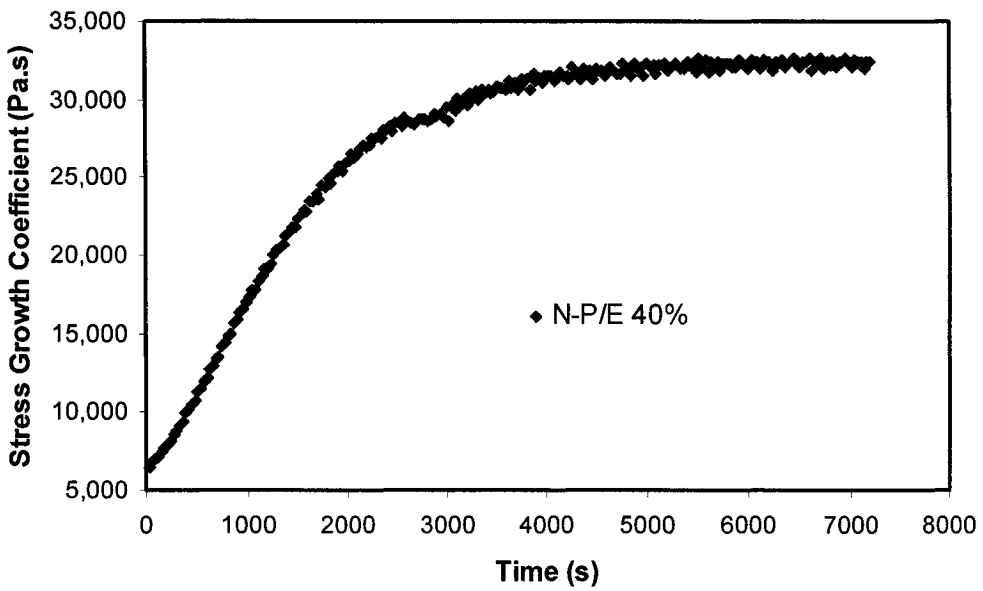

Figure 4.17 The time-dependent viscosity (N-P/E 40% $CaCO_3$ at T=160°C, $\dot{\gamma}$=0.001 s^{-1})

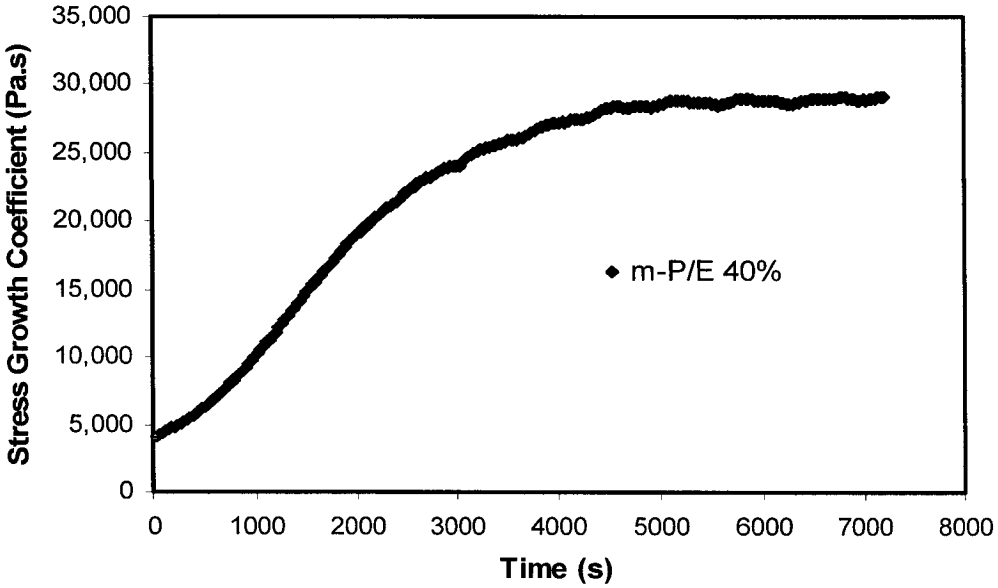

Figure 4.18 The time-dependent viscosity (m-P/E 40% $CaCO_3$ at T=160°C, $\dot{\gamma}$=0.001 s^{-1})

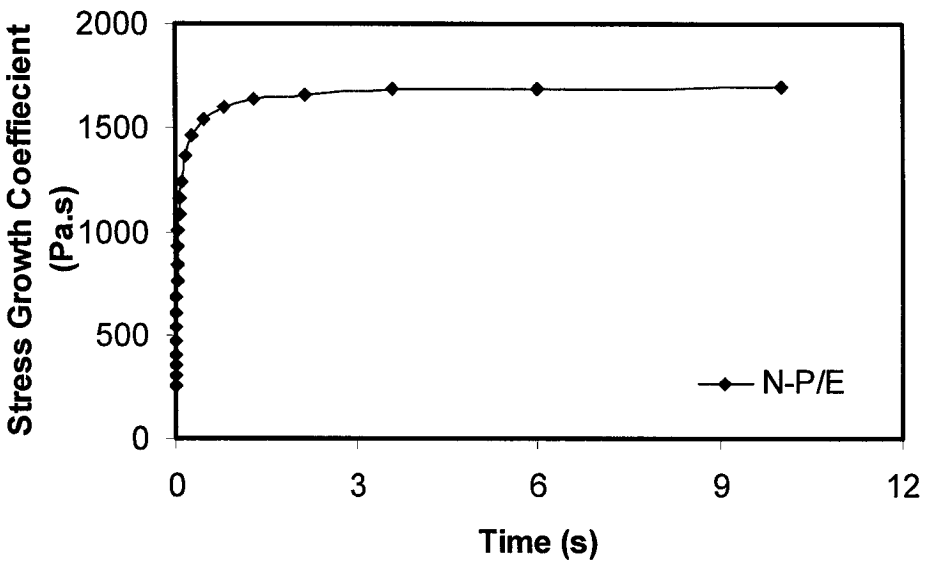

Figure 4.19 The time-dependent viscosity of N-P/E at T=160°C (Estimated from the complex viscosity assuming applicability of the first Gleissle mirror relation and Cox-Merz rule)

References

1. Zhu, K., *Thermorheology of Long Chain Branched Metallocene Polyethylene,* MASc. Thesis presented to Concordia University, 2003

2. Carreau, P. J., De Kee, D. C. R., and Chhabra, R. P., *Rheology of Polymeric Systems: Principles and Applications,* Hanser/Gardner, 1997

Chapter 5. Analysis and Discussion of Results

5.1 Morphology of Filled N-P/E Systems

Figure 5.1 shows the morphology of N-P/E 40% $CaCO_3$ and 60% $CaCO_3$ loadings. From the SEM images below we can know that:

- The filler particles are well dispersed in N-P/E matrix
- The particles have a very broad size distribution
- The clear interface shows the very weak particle-matrix adhesion

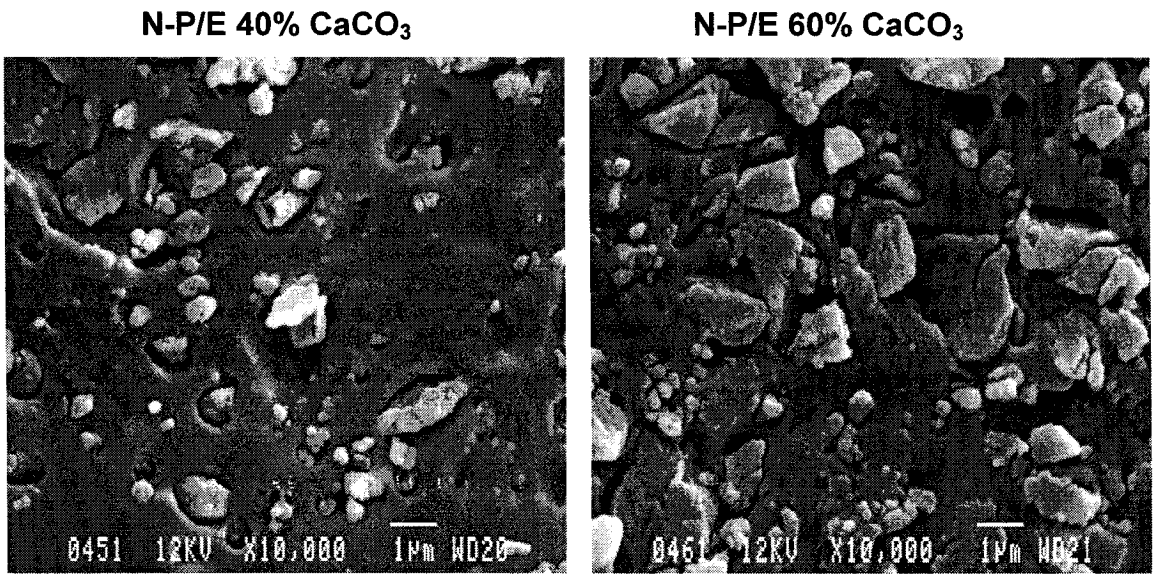

Figure 5.1 The SEM images of N-P/E 40% $CaCO_3$ and 60% $CaCO_3$

(Supplied by Dr. Luminita Ionescu)

In this work, $CaCO_3$ particles have a very broad size distribution from nano-scaled to several microns (Figure 4.2) which allows a higher maximum packing fraction. The particle surface is chemically coated with stearate at monolayer coverage. This organic hydrophobic coating layer decreases the particle-matrix adhesion. The reduced particle-

matrix interaction will lead to a lower onset stress σ_c of interfacial slip which may result in the reduced viscosity of the composite.

5.2 Thermorheology

5.2.1 Thermorheological Complexity

Time-temperature superposition is a well-known procedure used to determine the temperature dependence of polymer rheological behavior. Many polymers have simple temperature dependences described by a single time shift factor. But in some cases the effects of temperature can not be described by a single time shift factor.

A plotting method for detecting thermorheologically complex behavior was suggested by Wood-Adams and Costeux [1]. In this method, a plot of the magnitude of the complex modulus vs. the product of zero-shear viscosity and frequency is used to detect thermorheologically complex behavior. Figure 5.2 shows the master curve of m-P/E which exhibits the thermorheologically simple behavior. However, N-P/E exhibits the slightly complex behavior (Figure 5.3) and time-temperature superposition principle does not apply.

N-P/E is a new propylene-ethylene copolymer with a broad chemical composition distribution. A continuum of ethylene-enriched or ethylene poor fractions are present in this system. Due to the different properties of these compositions, certain molecular chains with enriched ethylene content may congregate which will lead to a thermorheologically complex behavior. M-P/E is a random propylene/ethylene copolymer, and ethylene is randomly distributed in the molecular structure, so no inhomogeneity is detected by the rheological test.

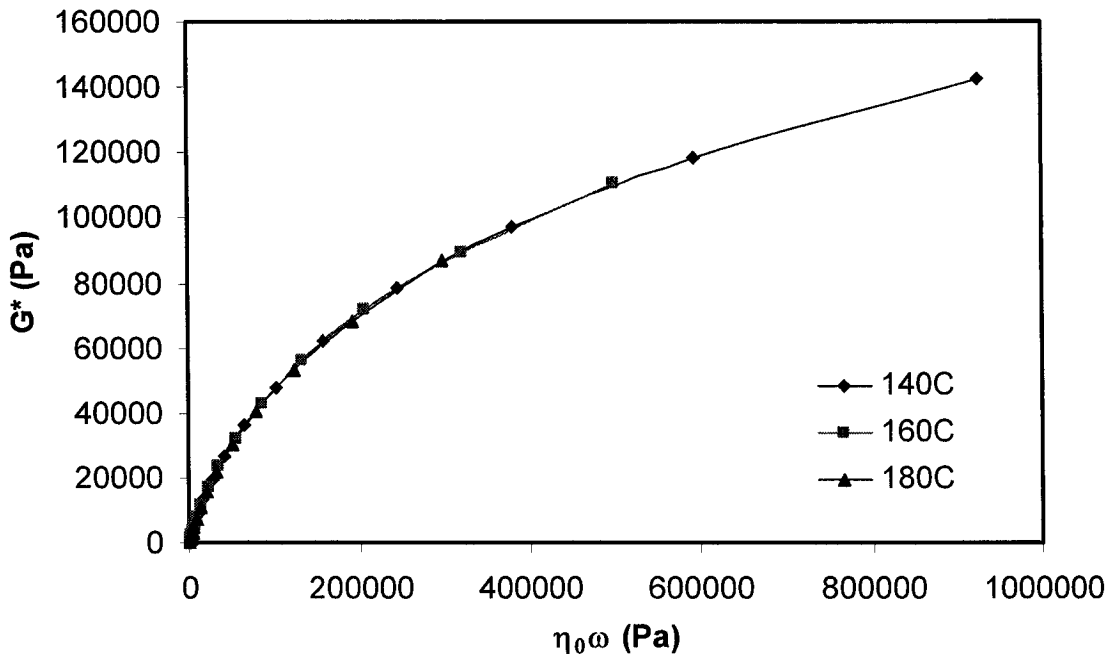

Figure 5.2 Thermorheologically simple behavior of m-P/E

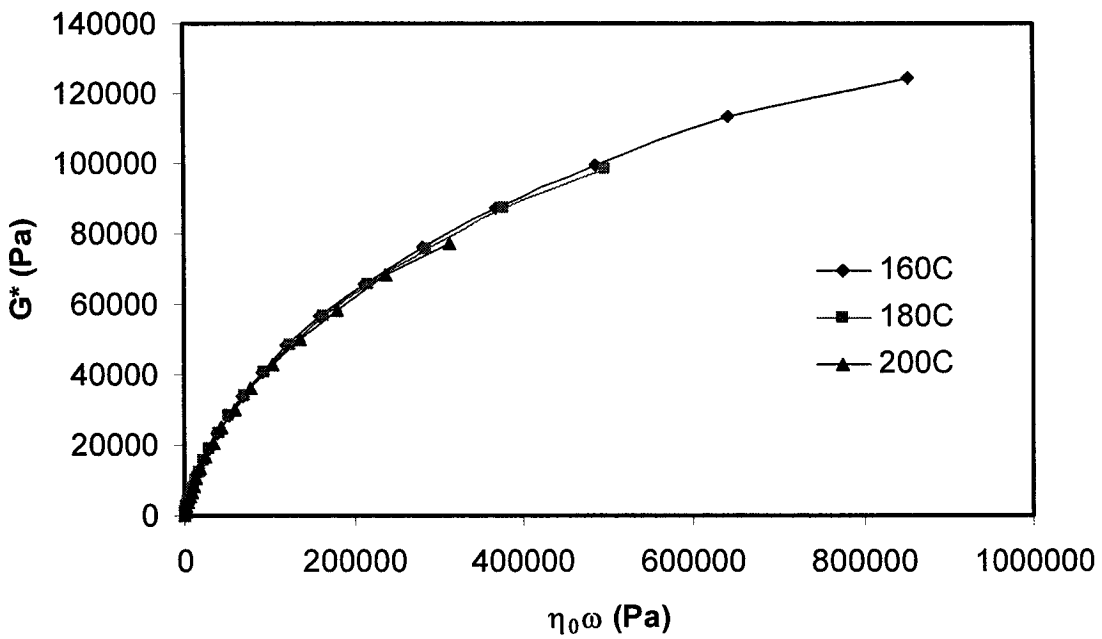

Figure 5.3 Thermorheologically complex behavior of N-P/E

5.2.2 Relaxation Spectrum

The relaxation spectrum, $H(\lambda)$, was calculated from $G'(\omega)$ and $G''(\omega)$ of the experimental materials using a nonlinear regularization technique [2]. Figures 5.4 and 5.5 and Figures 5.7 and 5.8 show the storage modulus and the loss modulus of N-P/E and m-P/E at different temperatures respectively. Figures 5.6 and 5.9 show the relaxation spectra of N-P/E and m-P/E at different temperatures. Since N-P/E has a relatively broader molecular weight distribution and a much broader chemical composition distribution, the relaxation spectrum of N-P/E exhibits a relatively broader distribution. Due to the temperature-dependent rheological properties, the N-P/E series have different shapes of relaxation spectrum which is an indicator of thermorheological complexity.

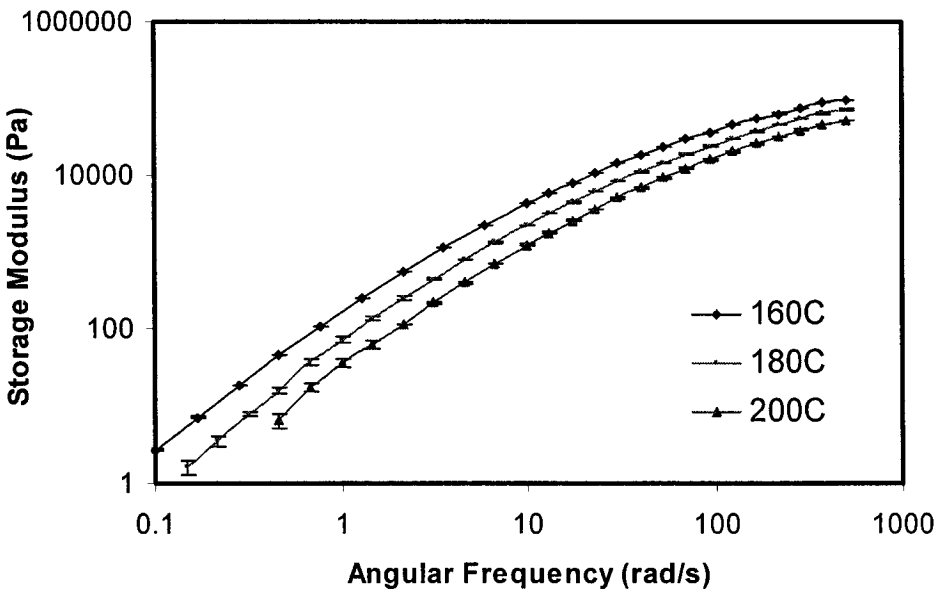

Figure 5.4 The storage modulus of N-P/E at 160, 180 and 200°C

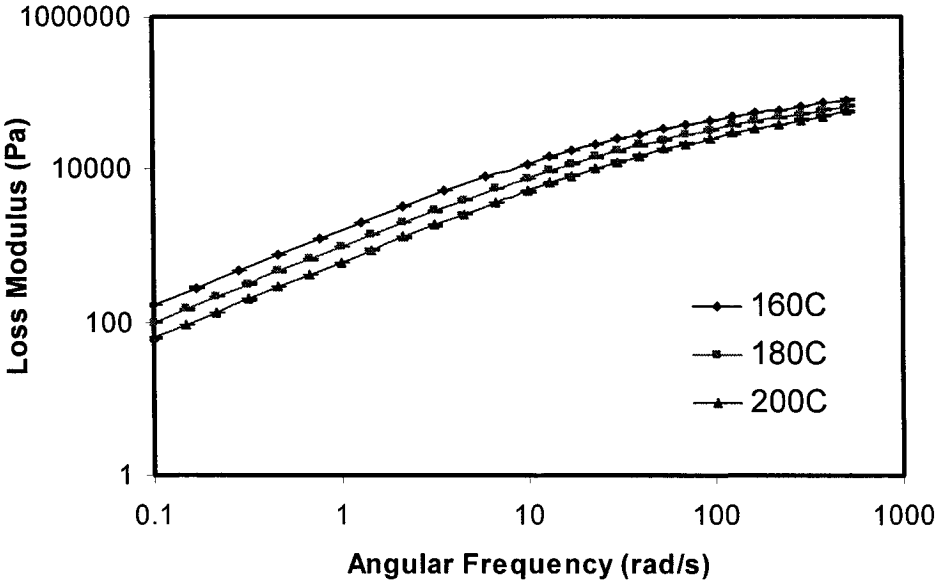

Figure 5.5 The loss modulus of N-P/E at 160, 180 and 200°C

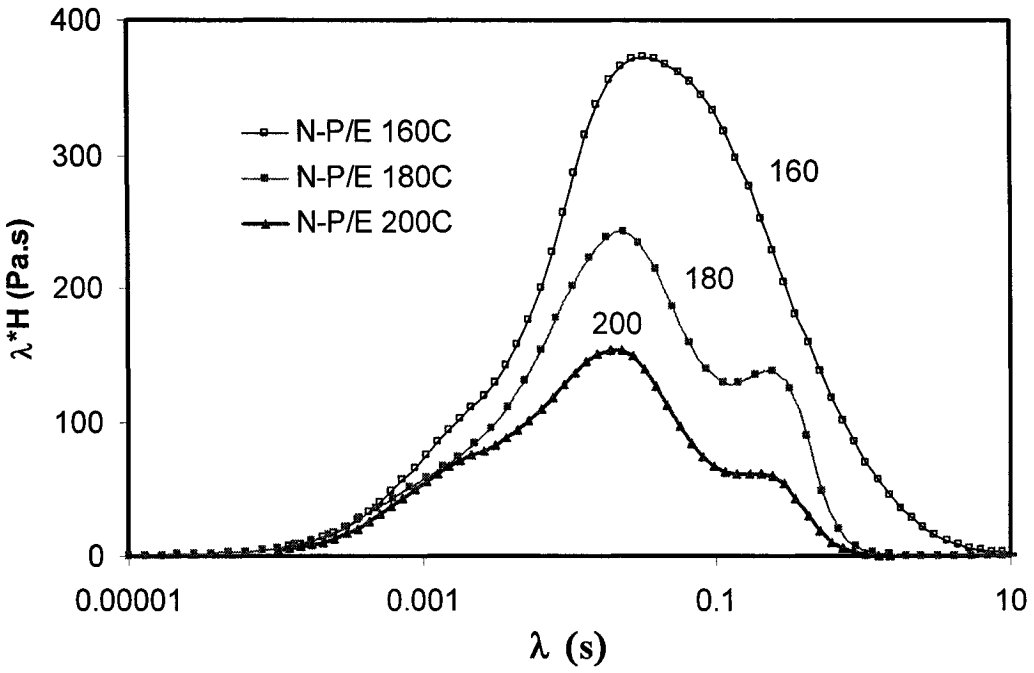

Figure 5.6 The relaxation spectrum of N-P/E at different temperatures

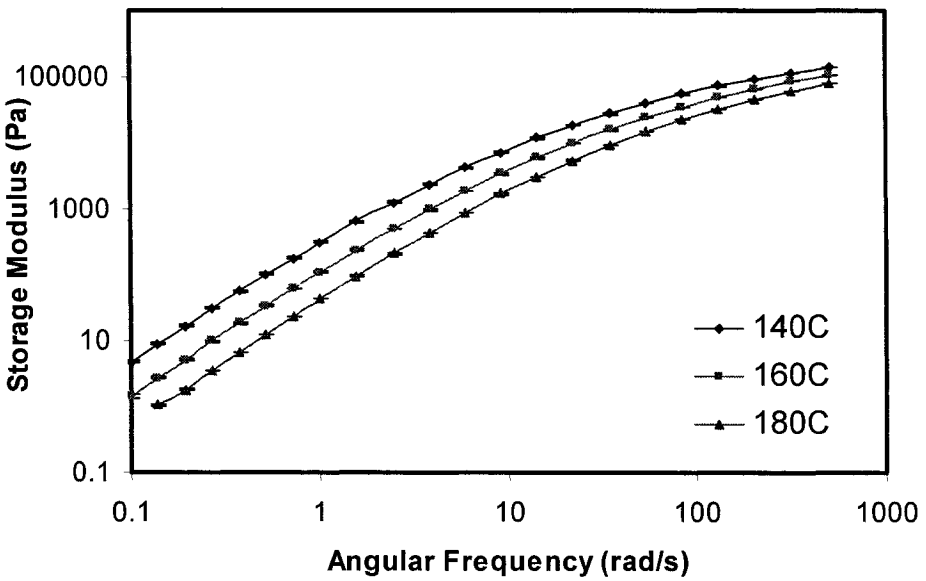

Figure 5.7 The storage modulus of m-P/E at 140, 160 and 180°C

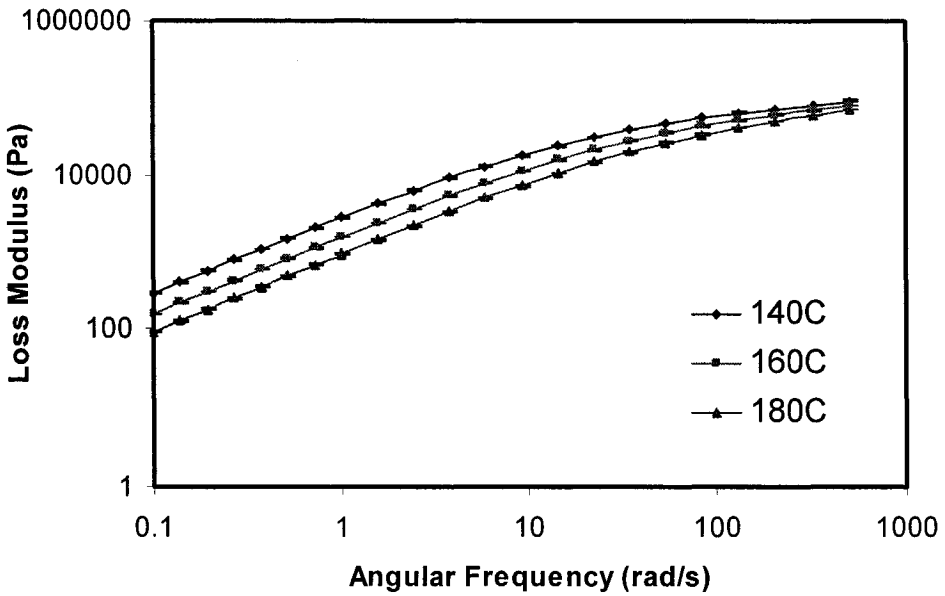

Figure 5.8 The loss modulus of m-P/E at 140, 160 and 180°C

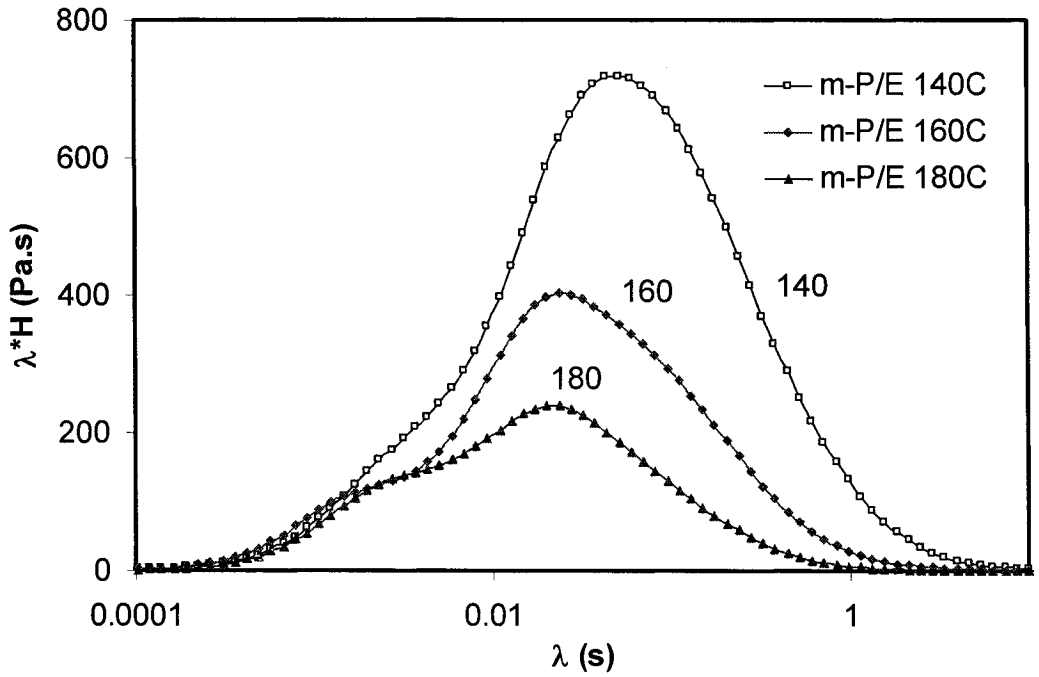

Figure 5.9 The relaxation spectrum of m-P/E at different temperatures

5.2.3 Flow Activation Energy

Usually rheological behaviors are highly temperature dependent. To fully understand the rheological behaviors of a particular material, experiments must be carried out at several temperatures [3]. Flow activation energy is a measure of temperature sensitivity of rheological material functions. Some materials exhibit thermorheologically simple behavior which can be displayed on the single master curve covering a much broader range of time at a single temperature. In this case the time shift factor α_T and the modulus shift factor b_T can be calculated by the equations below:

$$\eta_0(T) = \alpha_T(T) b_T(T) \eta_0(T_0) \tag{22}$$

$$G_N^0(T) = b_T(T) G_N^0(T_0) \tag{23}$$

Where T_0 is an arbitrary reference temperature.

According to the Arrhenius equation, $\alpha_T = \exp\left[\frac{E_a}{R}(\frac{1}{T}-\frac{1}{T_0})\right]$; And b_T is often neglected due to $b_T \approx 1$.

But for thermorheologically complex materials, the single activation energy can not fully represent the temperature dependency since the temperature sensitivity is time-dependent. In this work, the flow activation energy of N-P/E was calculated based on the storage modulus of experimental materials. Figure 5.10 is the activation energy spectrum at different relaxation times. Table 5.1 shows the activation energy of different polyolefins. We can find that the N-P/E has an activation energy ranging from 4500-6000 K (Ea/R). M-P/E has a single activation energy of Ea/R=5240K.

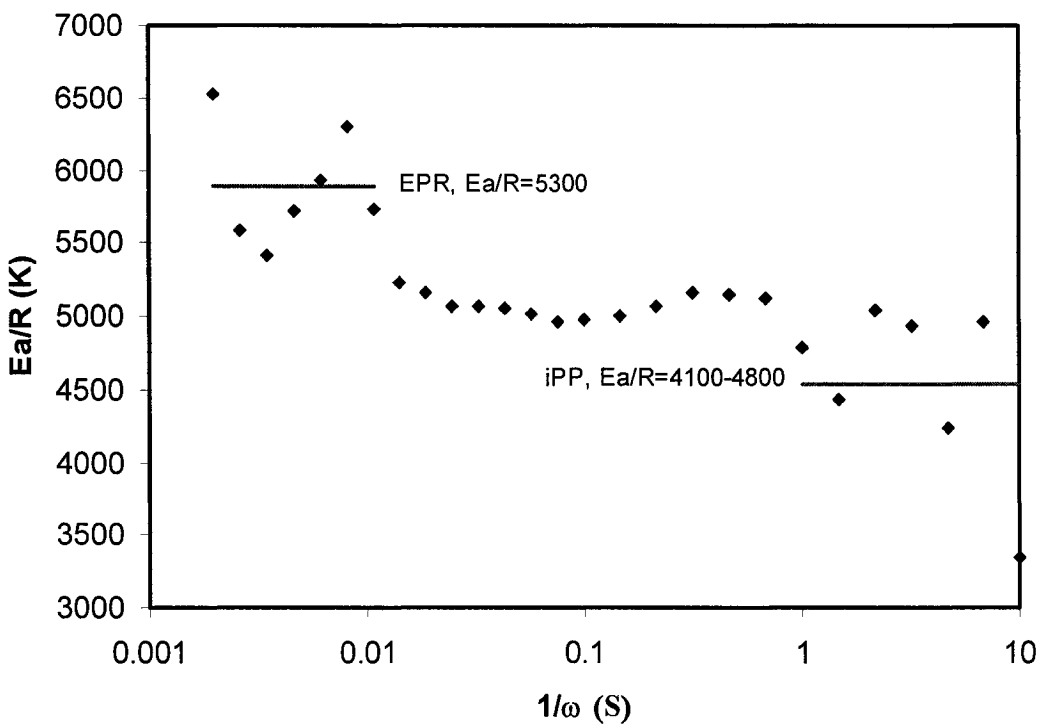

Figure 5.10 Flow activation energy spectrum of N-P/E (based on G')

Table 5.1 Flow activation energy of some polyolefins

Materials	Linear iPP [4]	EPR_{Ti}[4]	**m-P/E**
Activation Energy Ea/R (K)	4103	5309	5240

Figure 5.10 quantifies the temperature sensitivity of N-P/E with thermorheological complexity. From this figure we can find three regions with different temperature sensitivities. The short-time activation energy shows the temperature sensitivity of EPR (See table above). The medium-time activation energy is the same as the random propylene-ethylene copolymer. The long-time activation energy shows the activation energy of isotactic polypropylene. This activation energy distribution is also an indicator of thermorheologically complex behavior of N-P/E.

Table 5.1 lists the flow activation energy of some relevant polyolefins. Due to the broad chemical composition distribution, the activation energy spectrum of N-P/E exhibits a combination of the activation energy of iPP, EPR and m-P/E.

5.2.4 Detecting Ethylene-Enriched Molecular Chains

Thermorheological analysis is a powerful tool for detecting the information about polymer molecular structure. Generally, thermorheological complexity shows complex flow behaviors at different temperatures which are caused by the relaxation mechanisms of different temperature dependency [5]. Polyolefin blends (for example, PP/PE) are immiscible due to no specific attractions because of the lack of polarity and functionality which will cause the microphase separation in the melt state [6-7]. Since N-P/E copolymer has a very broad chemical composition distribution which means that it is a mixture of

different chemical compositions, zones of enriched ethylene content may be occurring in the melt state. The thermorheological complex behavior (Figure 5.3) gives indirect proof of inhomogeneity in the N-P/E melt. M-P/E is a metallocene-based propylene/ethylene copolymer which exhibits a thermorheologically simple behavior. We attribute the behavior to the narrow chemical composition distribution.

Different materials exhibit different relaxation mechanisms. From the relaxation spectra of N-P/E and m-P/E (Figure 5.6 and 5.9), we can find that N-P/E has a bimodal relaxation time distribution which is due to the combination of different relaxation mechanisms. Also the relaxation spectrum analysis provides another indirect proof of multiple relaxation mechanisms in the N-P/E melt.

Due to the different compositions, certain chains may congregate at the interface with the filler in the composites which may enhance interfacial slip under shear flow. Figure 5.11 shows the AFM phase images of m-P/E 20% $CaCO_3$ and another N-P/E copolymer with 20% $CaCO_3$ at a temperature of 80°C. We can find that all the filler particles in this new copolymer matrix are surrounded by amorphous region. However, only partial particles in m-P/E matrix are surrounded by the amorphous material. This leads to the better particle dispersion in the new P/E copolymer. Meanwhile it will also result in a reduced composite viscosity and enhance the particle-matrix interfacial slip.

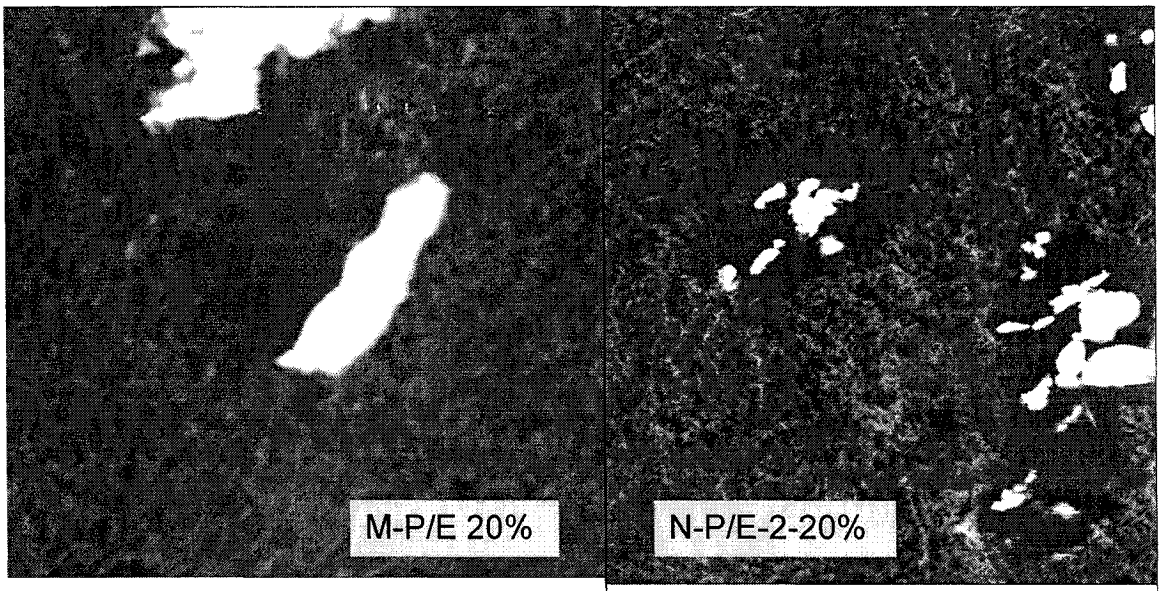

AFM phase images at 80°C
(Supplied by The Dow Chemical Company)

Figure 5.11 Effect of ethylene-enriched chains on viscosity

5.3 Steady-State Shear Viscosity

5.3.1 Steady-State Shear Viscosity

The steady-state shear viscosities were measured by plate-plate geometry on an Anton-Paar Physica stress-controlled rheometer. Figure 5.12 and 5.13 show the measured viscosities of N-P/E and m-P/E series. All the viscosities have been corrected by the method described in Chapter 4. Due to the bulk slip, the viscosities of samples with 80% loading can not be measured by regular rotational viscometry. The viscosities of samples with 60% loading above have been truncated at $\dot{\gamma}$ =0.5 s^{-1} because of unstable measurements at higher rates. From Figure 5.12 and 5.13 we can find that all the filled systems exhibit shear thinning behaviors and that the matrices are essentially Newtonian in this low shear rate region.

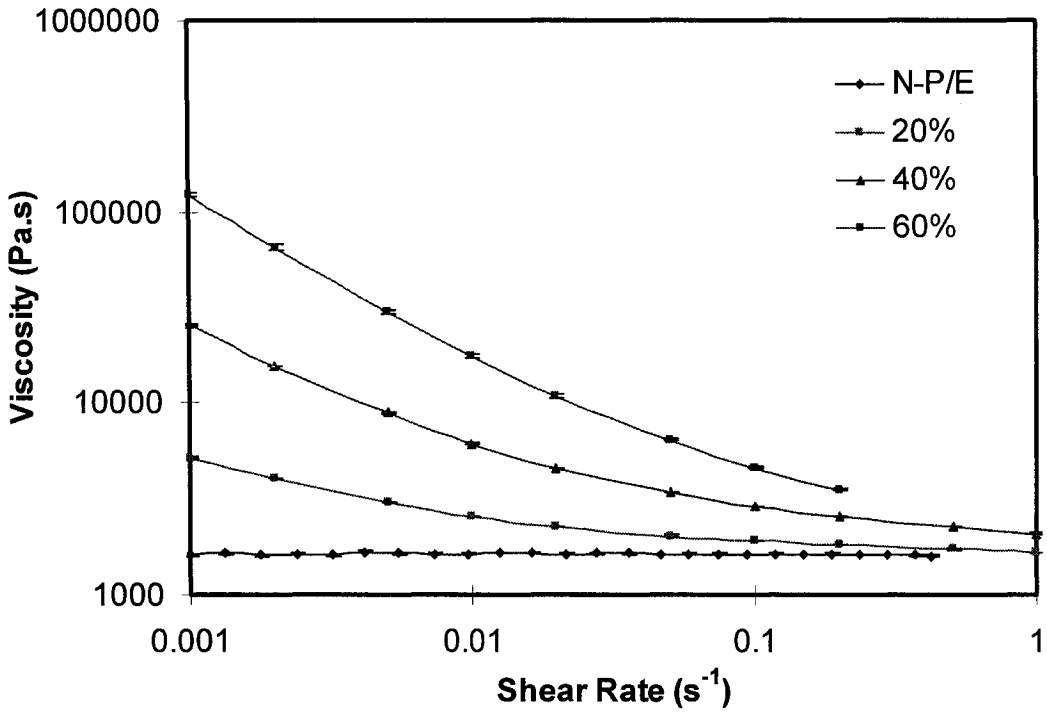

Figure 5.12 The viscosities of N-P/E Series at T=160°C

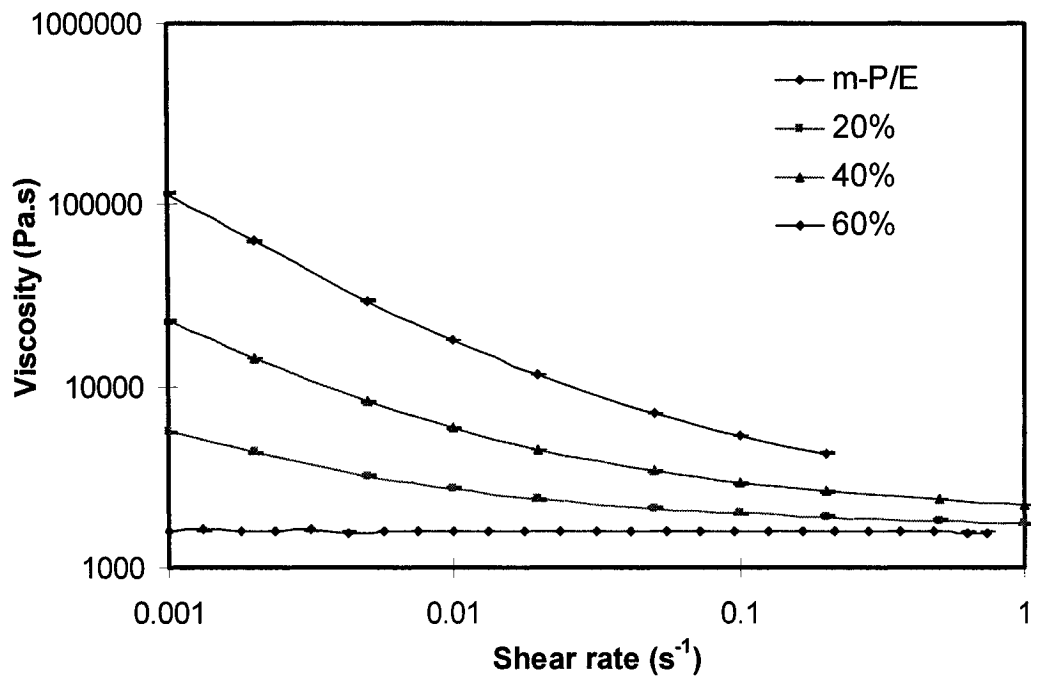

Figure 5.13 The viscosities of m-P/E series at T=160°C

Figure 5.14 shows the viscosity comparison of filled N-P/E and m-P/E series. From Figure 5.14 we can find that at high rates the m-P/E composites have higher viscosities.

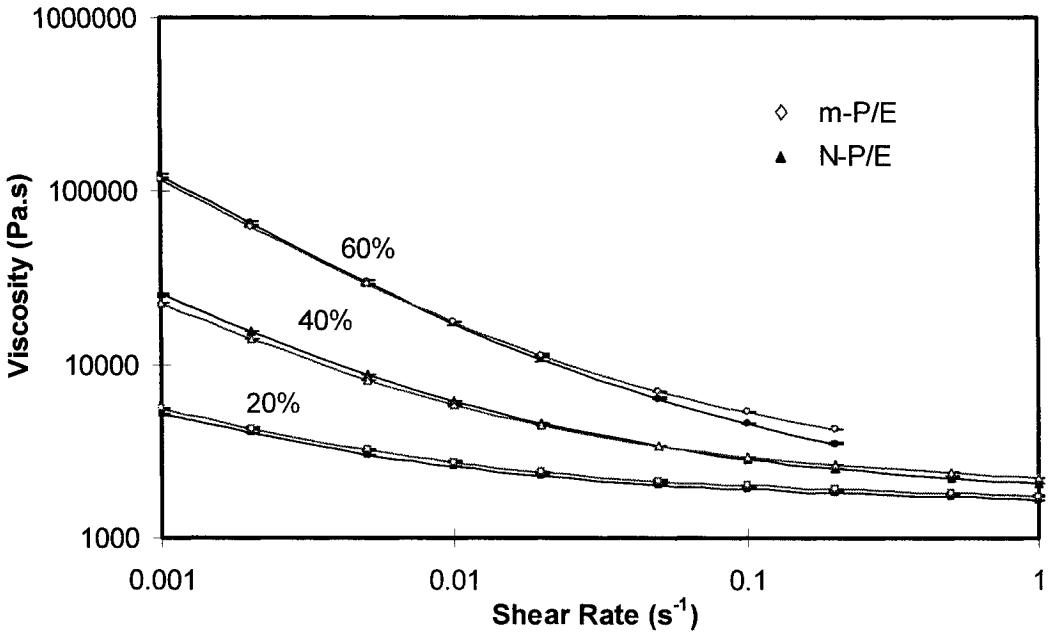

Figure 5.14 Viscosity comparisons of N-P/E and m-P/E series at T=160°C

5.3.2 Relative Viscosity

Relative viscosity is the ratio of the viscosity of the filled polymer suspension to that the pure polymer either at constant shear rate or at constant shear stresses.

$$\eta_{r(\dot{\gamma}/\sigma)} = \eta_{(\phi)} / \eta_m \tag{24}$$

Where η_r is the relative viscosity. $\eta_{(\phi)}$ is the viscosity of the suspension with a filler volume fraction ϕ. η_m is the viscosity of pure resin. In this work, the relative viscosities were calculated both at constant shear rates and constant shear stress, and Figure 5.15 shows the relative viscosities of N-P/E and m-P/E series at $\dot{\gamma}$ of 0.001 s^{-1}. Figure 5.16 shows the relative viscosities of N-P/E and m-P/E series at $\dot{\gamma}$ of 0.2 s^{-1}. The relative

viscosities of N-P/E series are slightly higher than m-P/E series at $\dot{\gamma}$ of $0.001s^{-1}$. However the relative viscosities of N-P/E series are much lower than m-P/E series at $\dot{\gamma}$ of $0.2s^{-1}$. The same results are given by the relative viscosities based on constant shear stress (Figure 5.17).

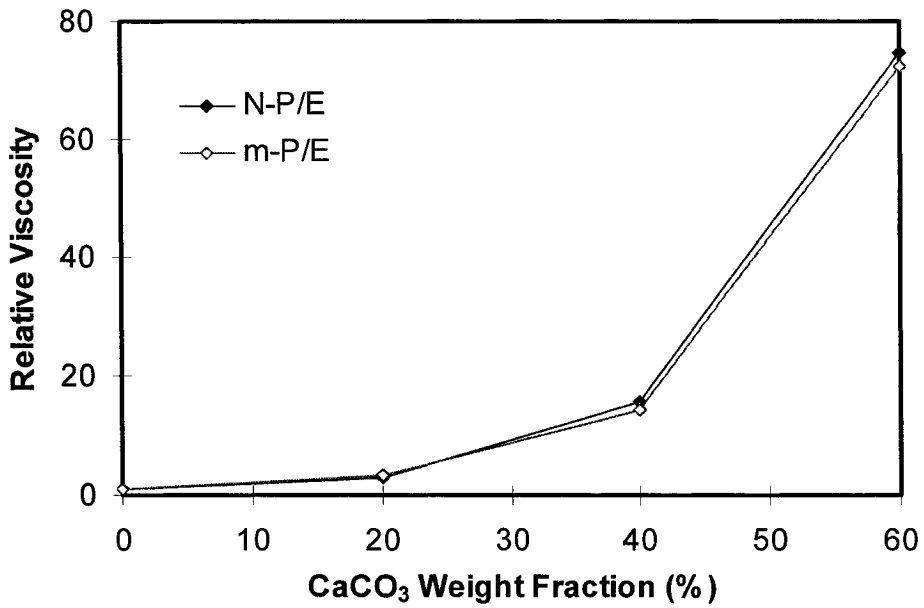

Figure 5.15 The relative viscosities of N-P/E and m-P/E series at $\dot{\gamma}$=0.001 s^{-1} at T=160°C

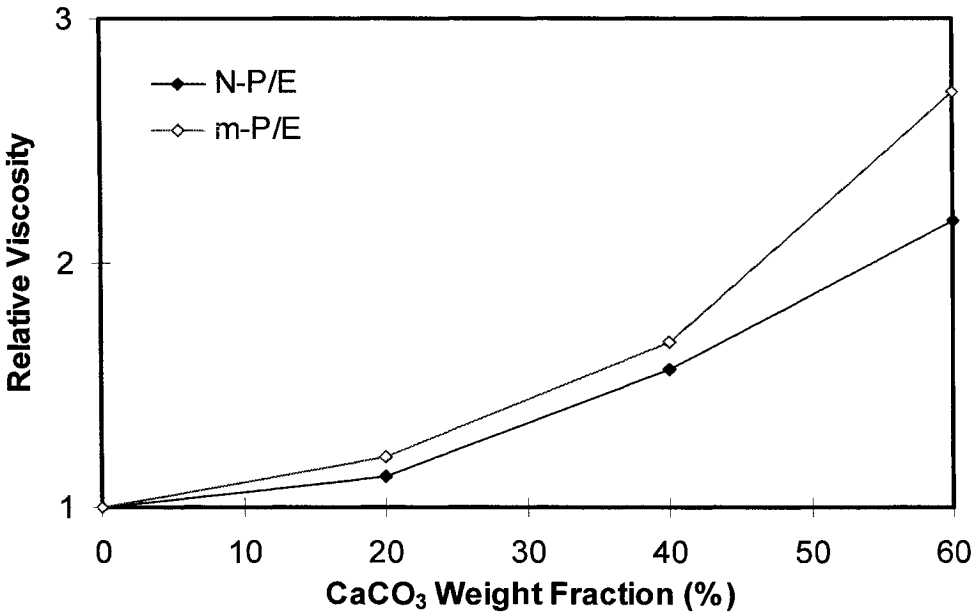

Figure 5.16 The relative viscosities of N-P/E and m-P/E series at $\dot{\gamma}$=0.2 s^{-1} at T=160°C

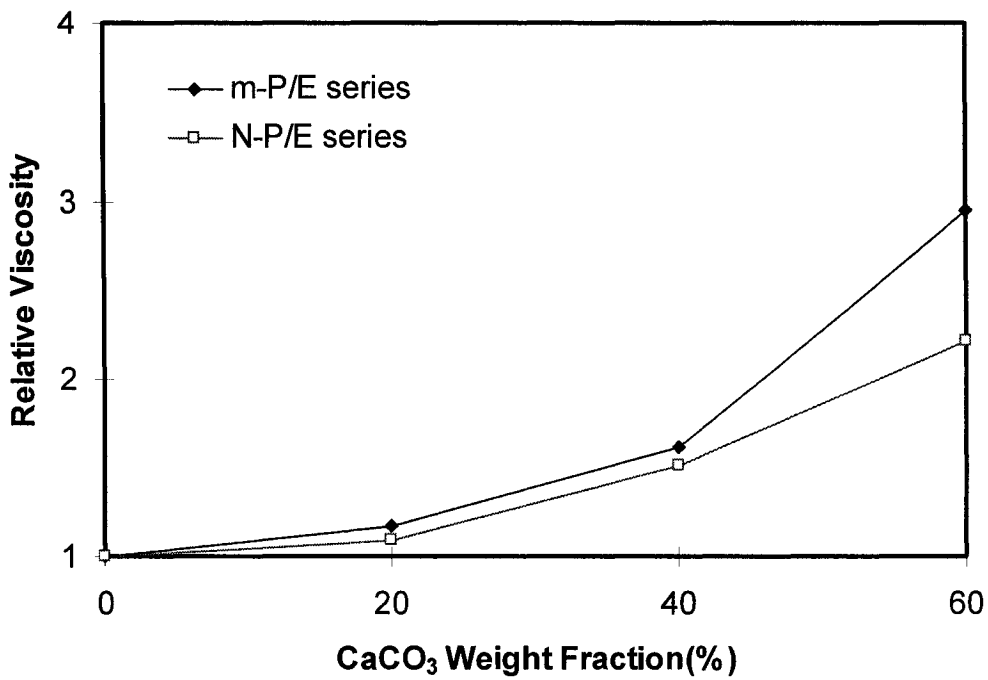

Figure 5.17 The relative viscosities of N-P/E and m-P/E series at shear stress of 700Pa and at T=160°C

5.3.3 Interfacial Slip (The Modified Einstein Equation)

The simplest multiphase system is the dilute suspension in a Newtonian fluid with non-deforming monosized spheres that do not experience Brownian motion. The shear viscosity $\eta(\phi)$ can then be predicted simply by the Einstein formula:

$$\eta_r = 1 + 2.5\phi \tag{25}$$

Where η_r is the relative viscosity defined in Equation 24 and ϕ is the volume fraction, and $\eta_r = \eta(\phi)/\eta_m$.

Since particle-matrix interfacial adhesion greatly affects the rheological behavior of multiphase systems, under a high enough shear stress, interfacial slip may be occurring. In the case of interfacial slip, the modified Einstein formula applies [8]:

$$\eta_{(\phi)} = \eta_m \left[1 + \frac{5(1+2b/R)}{2(1+5b/R)}\phi \right] \tag{26}$$

In case of complete slip, $b >> R$, $$\eta(\phi) = \eta_m(1+\phi) \tag{27}$$

In case of no slip, b =0, and $$\eta(\phi) = \eta_m\left(1+\frac{5}{2}\phi\right) \tag{28}$$

Where R is the sphere radius, η_m is the medium viscosity, b is the extrapolation length characterizing the sphere-medium interfacial interactions, and $\eta_r = \eta_{(\phi)}/\eta_m$ is the relative viscosity. Upon applying a high enough stress, sufficient chain desorption takes place instantaneously to cause interfacial slip and results in reduced viscosity. Figure 5.18 shows the effect of interfacial slip on the relative viscosities. In this work, the volume fraction of particles was calculated in the melt state. The specific density of $CaCO_3$ is 2.7g/cm^3 and the thermal expansion coefficient of N-P/E and m-P/E (all polyolefins have

a similar thermal expansion coefficient) is 13×10^{-5}cm/cm°C. Since the thermal expansion coefficient of $CaCO_3$ is very small, it will be neglected in the calculation. The densities of N-P/E and m-P/E are 0.8671g/cm^3 and 0.8864g/cm^3 respectively at room temperature. Table 5.2 lists the calculated volume fractions of filler particles in different copolymers.

Table 5.2 Filler volume fractions at 160°C

Filler Loading, wt%	20	40	60	80
Filler Volume Fraction in N-P/E v%	7.08	16.89	31.37	54.94
Filler Volume Fraction in m-P/E v%	7.22	17.20	31.85	55.48

Figure 5.18 shows the effect of interfacial slip on the relative viscosities of two sets of materials at shear stress of 700Pa. We can find that N-P/E series have lower relative viscosities due to stronger interfacial slip. The slip lengths of filled systems under shear were listed in Table 5.3 which were calculated based on the modified Einstein equation. Partial slip was detected in N-P/E 20%; and almost no slip was detected in m-P/E 20%. For the filled systems with higher loadings, the modified Einstein equation did not apply because of the strong particle-particle interactions.

Figure 5.19 shows the slip transition on the particle-matrix interface. From this figure we can find that the interfacial slip of N-P/E 20% experiences a clear transition. The slip length is almost constant at low stress. At the stress of about 100 Pa, the slip length starts to increase sharply with stress. Since the limited stress (shear rate) for the plate-plate geometry, we can not achieve the total transition process. However, almost no slip

transition can be achieved in m-P/E 20% across the full experimental window. In this figure the negative slip length is due to the shear-induced particle-particle interaction.

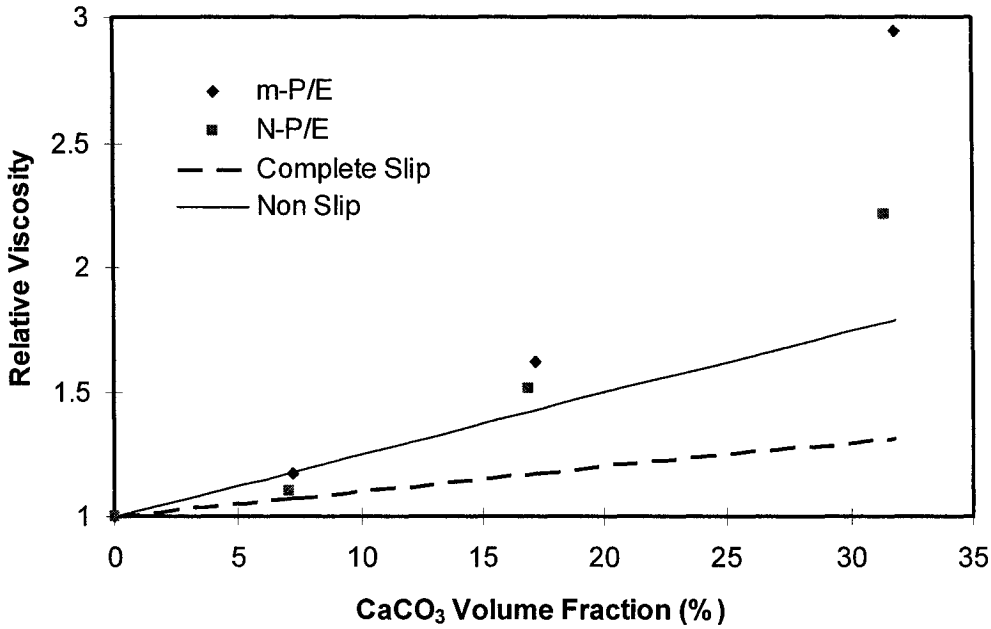

Figure 5.18 Effect of interfacial slip on relative viscosities at shear stress of 700Pa

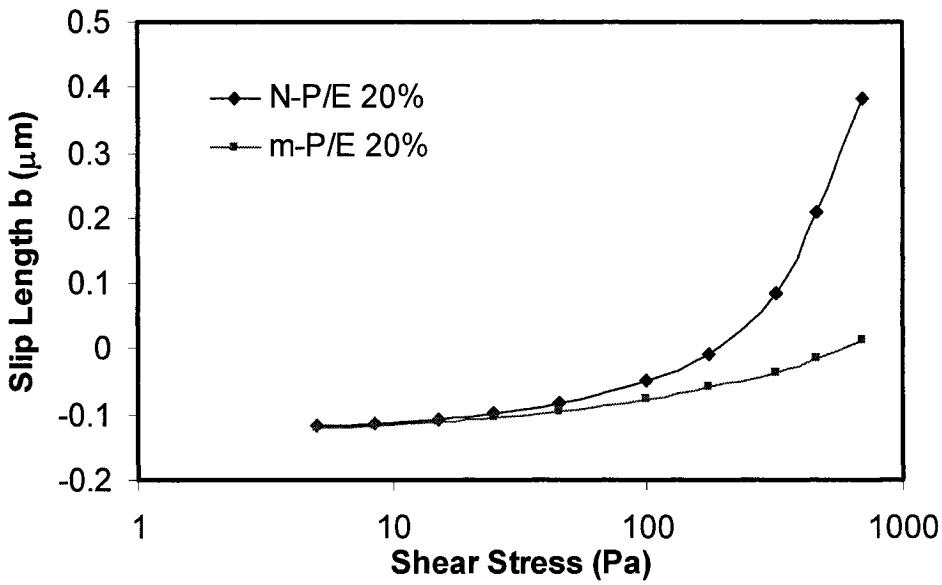

Figure 5.19 Slip transition on particle-matrix interface

Table 5.3 Slip Length at shear stress of 700 Pa

Filled Systems	m-P/E 20% $CaCO_3$	N-P/E 20% $CaCO_3$
Slip Length	0.014μm	0.370 μm

The Maron and Pierce empirical equation [9] is often used to predict the viscosity behavior of concentrated suspensions.

$$\eta_r = \left[1 - \frac{\phi}{\phi_m}\right]^{-2} \tag{29}$$

We can fit our experimental data to this equation and the maximum packing fraction can be calculated at each shear stress. However, it must be noted that the Maron and Pierce equation only applies with non-interactive particles. In our case this equation is meaningless due to the shear-induced particle-particle interaction and particle-matrix interfacial slip at high shear stress.

5.4 Linear Viscoelasticity of Filled Systems

5.4.1 Relaxation of Molding Induced Structure

The experimental samples were prepared by compression molding. Because of the agglomeration and orientation of particles caused by hot-pressing, the resulting structure will relax when they are loaded in rheometer. Usually the relaxation mechanism is very complicated and is influenced by many factors like particle motion, interfacial interaction and matrix properties. In this work, the oscillatory time sweep is used to monitor the microstructure evolution in the melt state.

Figure 5.20 shows the time sweep of N-P/E 20% at frequency=1 s^{-1}, γ=0.1% and T=160°C which exhibits a decreasing complex viscosity with time. However, m-P/E 20% has an increasing complex viscosity (Figure 5.21) under the same conditions.

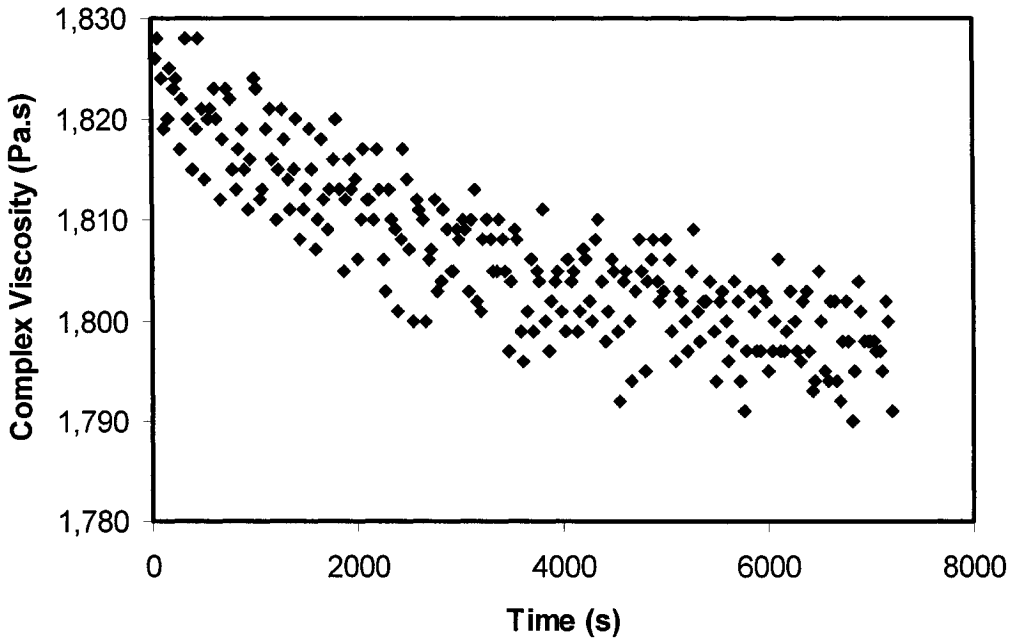

Figure 5.20 The time sweep of N-P/E 20% $CaCO_3$ at frequency=1 s^{-1}, γ=0.1%, T=160°C

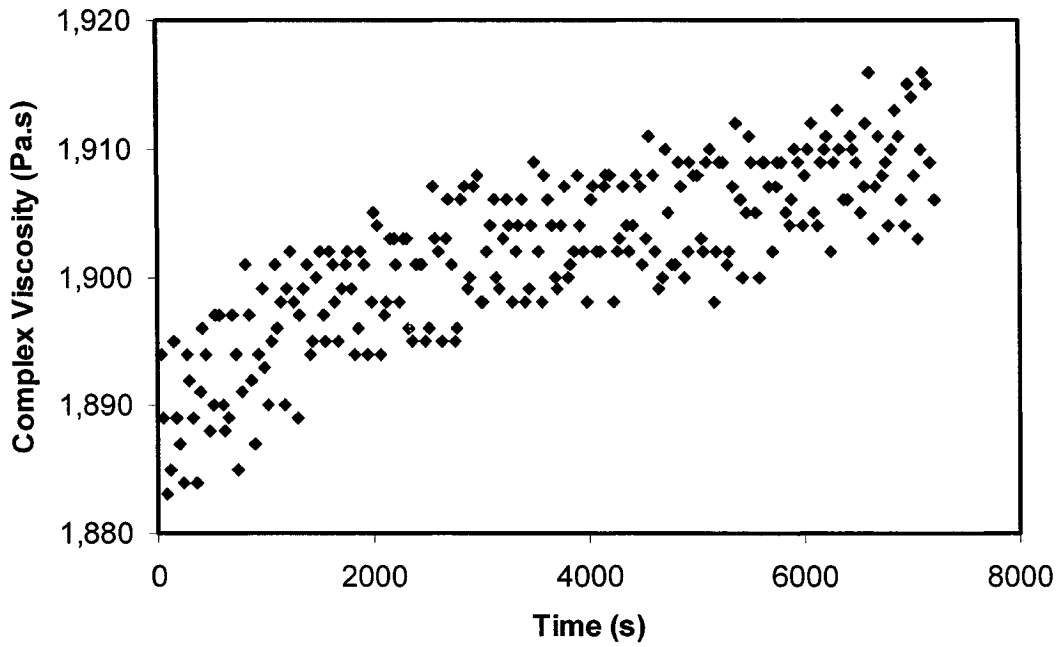

Figure 5.21 The time sweep of m-P/E 20% $CaCO_3$ at frequency=$1s^{-1}$, γ=0.1%, T=160°C

N-P/E is a propylene/ethylene copolymer with a broad chemical composition distribution. The enrichment of high ethylene content chains on the particle surface decreases the particle-matrix adhesion and makes the particles rotate freely in the melt in response to Brownian motion. Figure 5.22 shows a schematic of the particle rotation in the melt state. In the case of free rotation of particles, no particle contact occurs when the particle volume fraction is lower than a critical value ϕ_c.

M-P/E is a propylene/ethylene copolymer with a narrow chemical composition distribution. Stronger particle-matrix adhesion prevents the particles from freely rotating in the melt. In this case, particle-particle interaction (cohesion) dominates the morphology of the multiphase system.

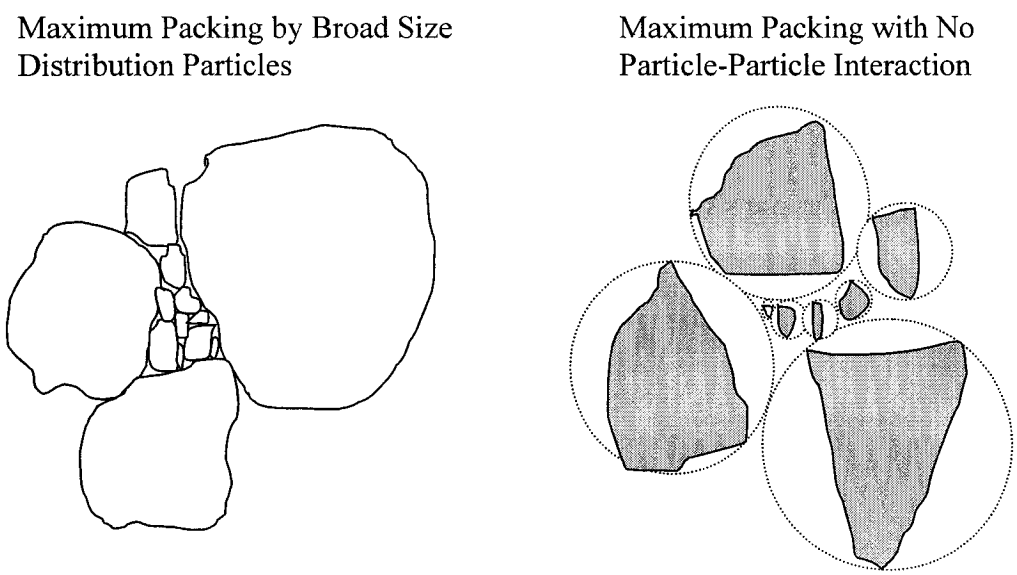

Figure 5.22 Maximum packing with no particle-particle interaction

Figure 5.23-5.26 show the time sweeps of N-P/E and m-P/E with higher filler loadings. They all exhibit a similar relaxation behavior. The complex viscosities increase with time and reach an equilibrium state after oscillatory shear for a period of long time. Due to the higher filler loading, contact-free rotation does not occur resulting in the increasing complex viscosities with time.

At lower volume fraction and low particle-matrix adhesion, the free rotation leads to a better dispersion of particles. But at higher volume fraction and strong interfacial adhesion, the particles tend to agglomerate. Because of the time-dependent structure of materials, all our oscillatory tests were performed after the stable structure was achieved.

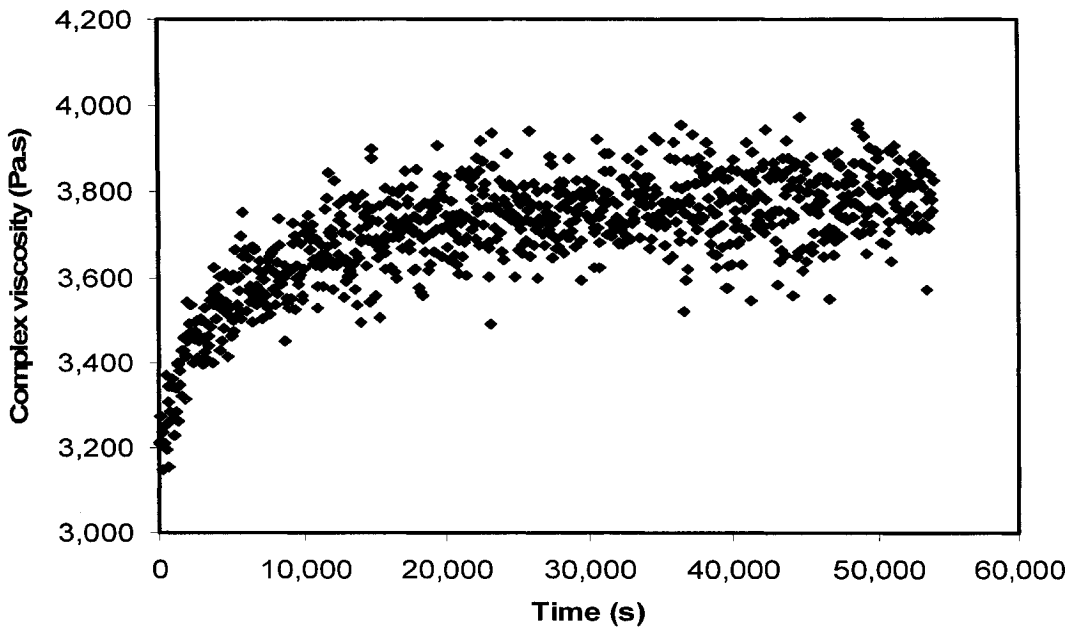

Figure 5.23 The time sweep of N-P/E 40% $CaCO_3$ at frequency=1 s^{-1}, γ=0.005%, T=160°C

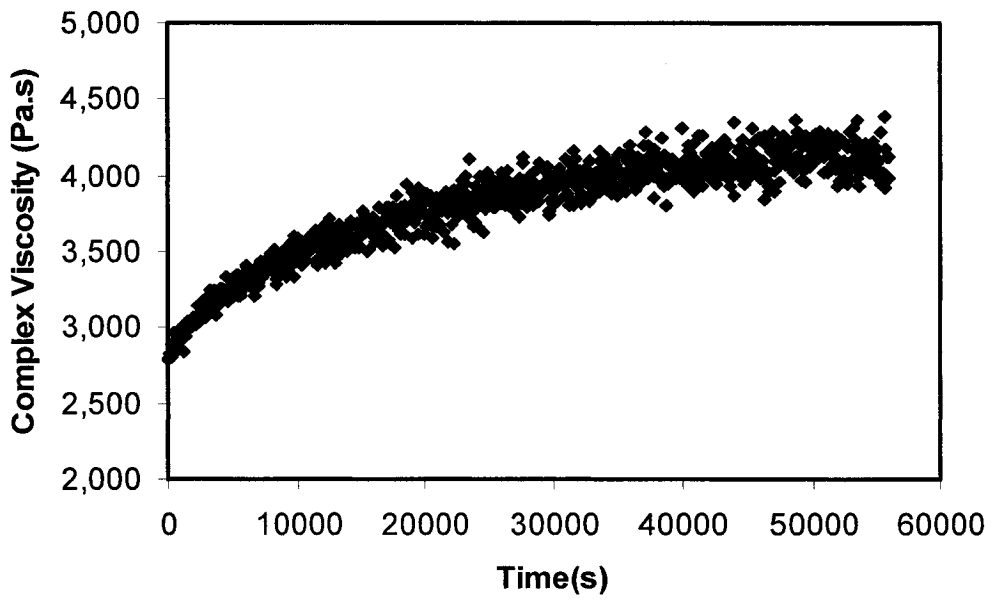

Figure 5.24 The time sweep of m-P/E 40% $CaCO_3$ at frequency=1 s^{-1}, γ=0.005%, T=160°C

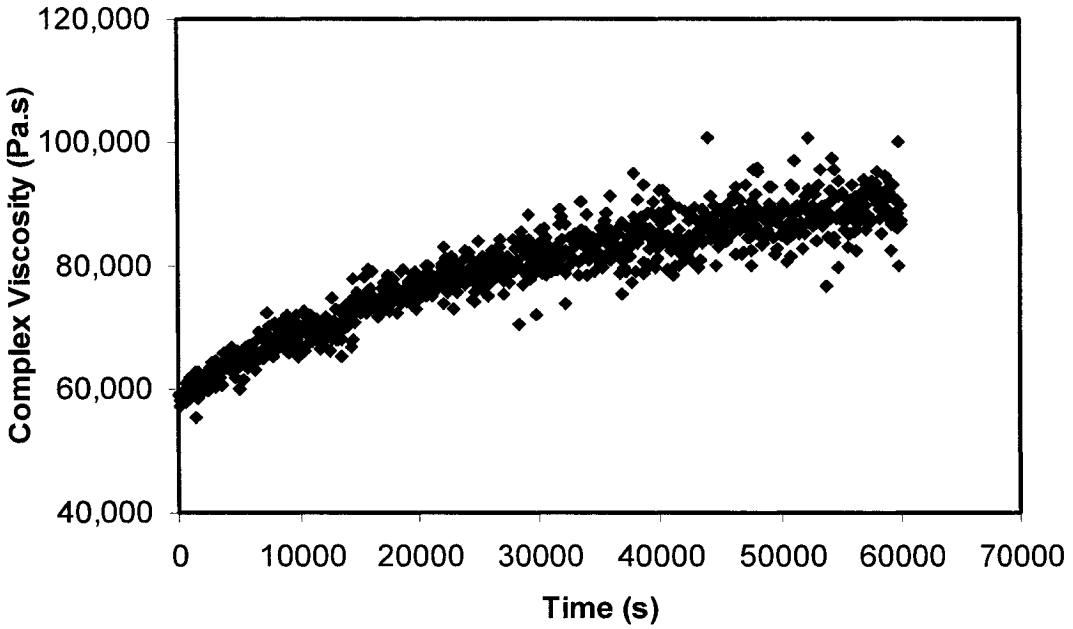

Figure 5.25 Time sweep of N-P/E 60% $CaCO_3$ at frequency=1 s^{-1}, γ=0.005%, T=160°C

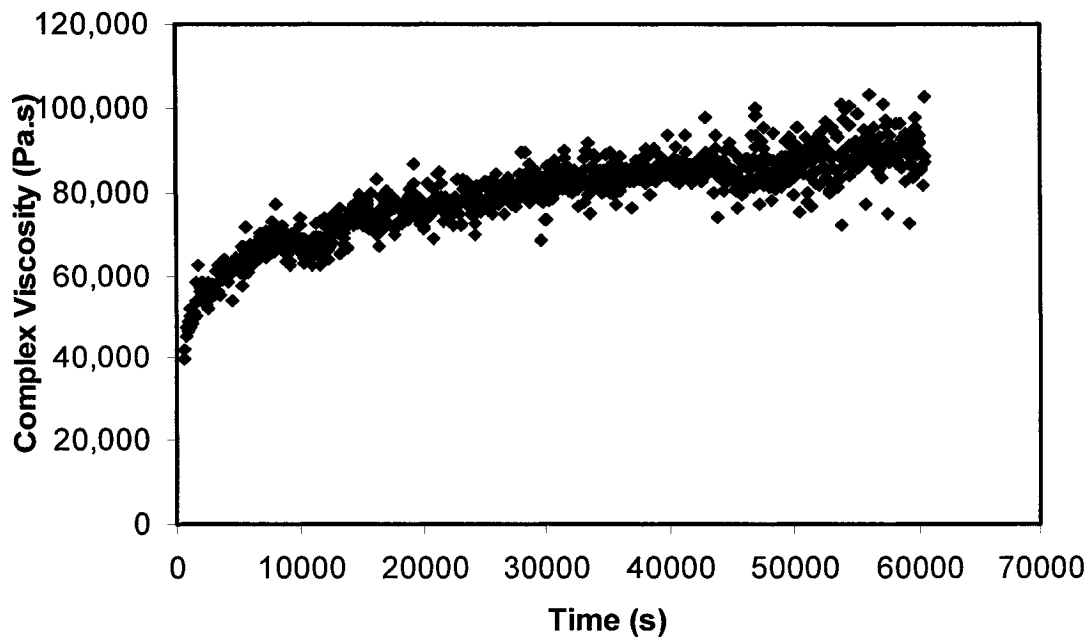

Figure 5.26 The time sweep of m-P/E 60% $CaCO_3$ at frequency=1 s^{-1}, γ=0.01%, T=160°C

5.4.2Complex Viscosity

Figure 5.27 and 5.28 show the complex viscosities of N-P/E and m-P/E series. Due to the relatively high viscosities of N-P/E and m-P/E with 40% and 60% loadings, we can not reach the Newtonian plateau in the oscillatory test range.

From Figure 5.27 and 5.28 we can find that filler content greatly affects the complex viscosities of materials. Figure 5.29 show the comparison of complex viscosities of N-P/E and m-P/E series. We can find that the m-P/E series exhibits higher complex viscosities at each filler content.

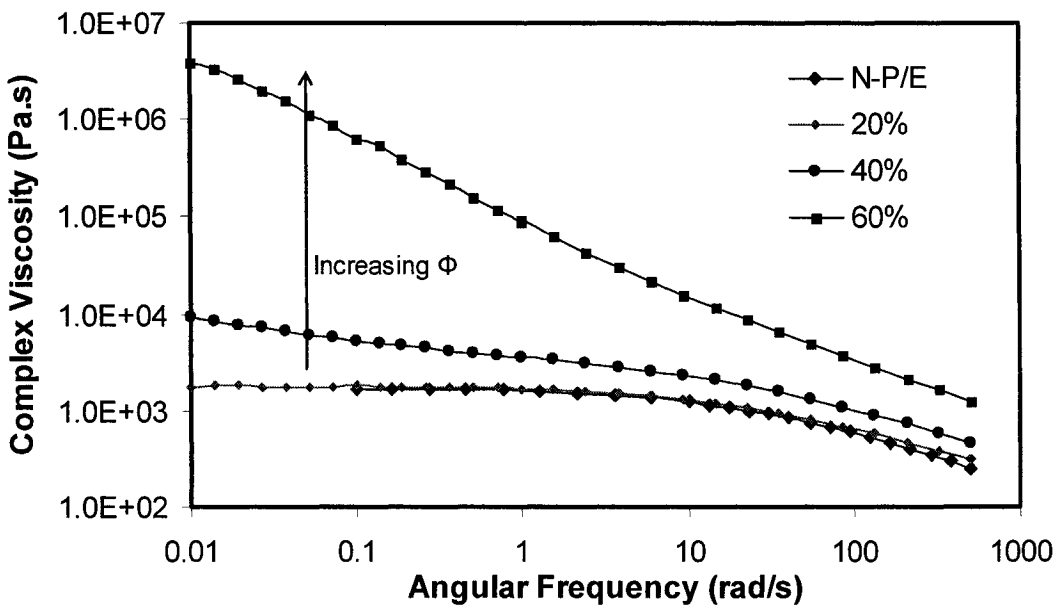

Figure 5.27 The complex viscosities of N-P/E series at T=160°C

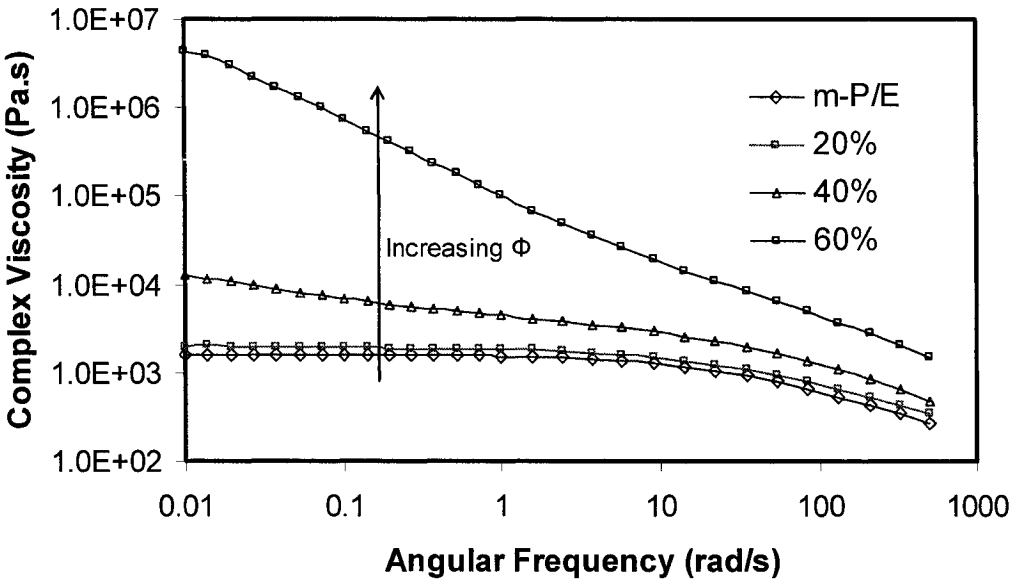

Figure 5.28 The complex viscosities of m-P/E series at T=160°C

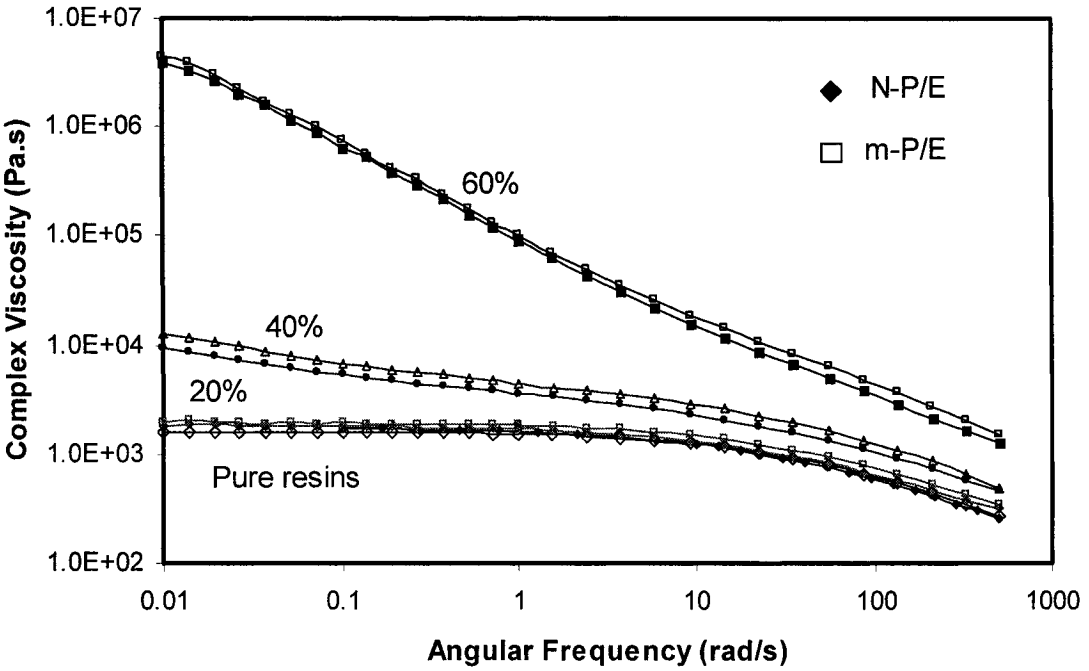

Figure 5.29 The complex viscosity comparison of N-P/E and m-P/E series at T=160°C

5.4.3 Storage Modulus

Storage modulus is an indicator of elastic properties of materials. Figure 5.30 and 5.31 list the storage modulus of N-P/E and m-P/E series. Due to the high loadings of particles, N-P/E and m-P/E with 60% loading are solid-like at low frequency.

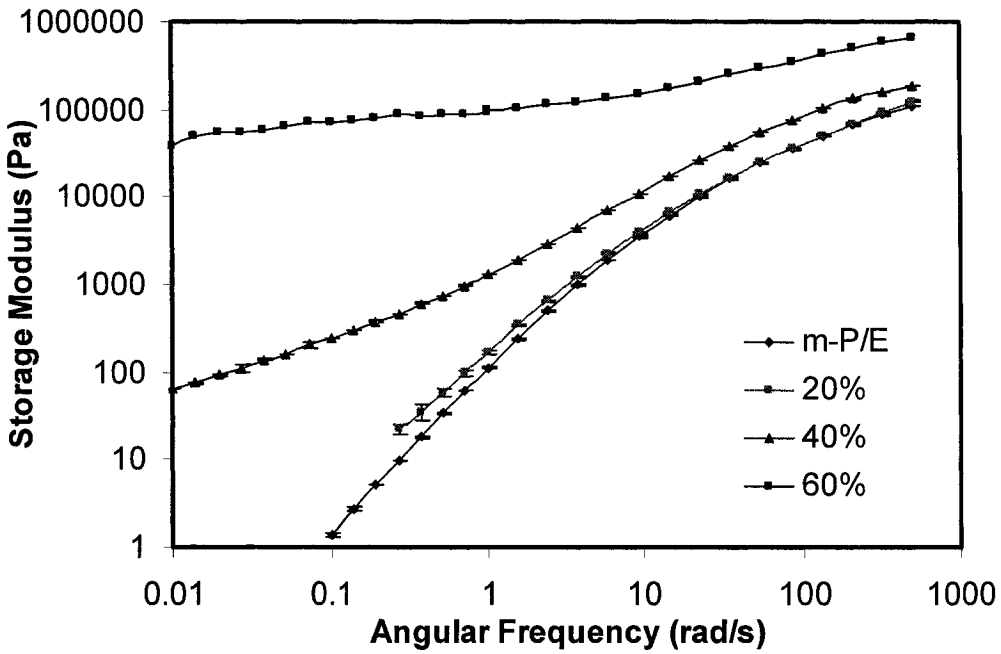

Figure 5.30 The storage modulus of m-P/E series at T=160°C

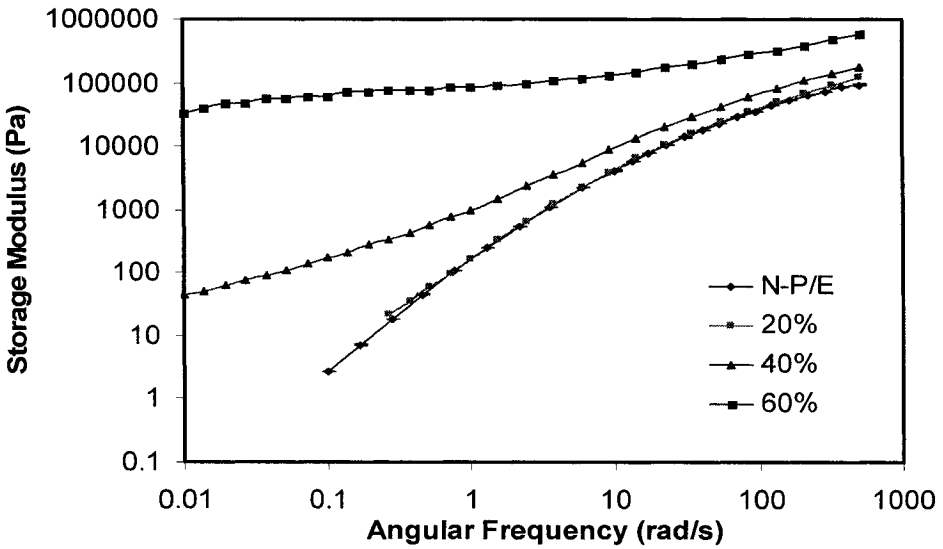

Figure 5.31 The storage modulus of N-P/E series at T=160°C

5.4.4 Loss Modulus

Loss modulus is an indicator of viscous properties of materials. Due to the solid-like properties of N-P/E and m-P/E with 60% loadings, the loss modulus at low frequency tends to be constant.

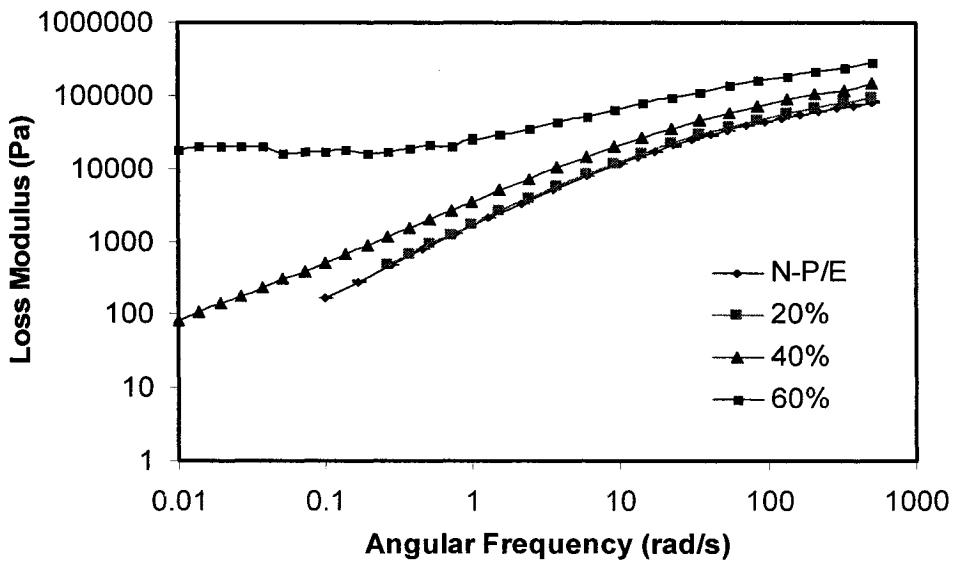

Figure 5.32 The loss modulus of N-P/E series at T=160°C

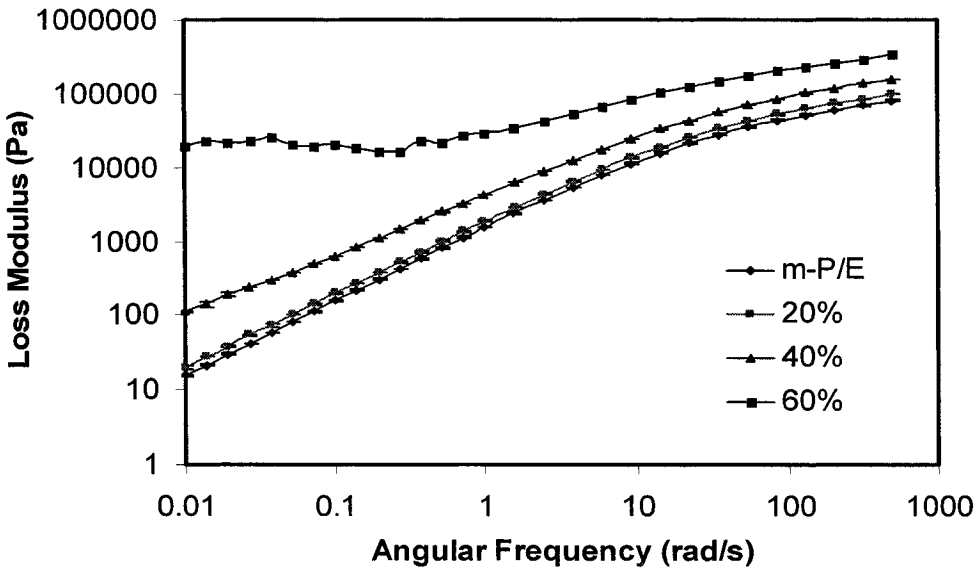

Figure 5.33 The loss modulus of m-P/E series at T=160°C

5.4.5 Effects of Filler Volume Fractions

From the storage modulus of N-P/E and m-P/E series, we can find that all the curves of the storage modulus at low frequency tend to be a straight line with a particular slope. The slopes of filled systems decrease with the increasing filler loading. To evaluate the effects of filler loadings on the linear viscoelasticity of filled systems, we make some plots of $\log(G')$ vs. $\log(\omega)$ and $\log(G'')$ vs. $\log(\omega)$ at low frequency. Figure 5.34 and 5.35 show the plots of $\log(G')$ vs. $\log(\omega)$ for m-P/E and N-P/E series at low frequency respectively. The slope δ is calculated by linear curve fitting. Figure 5.36 and 5.37 show the plots of $\log(G'')$ vs. $\log(\omega)$ for m-P/E and N-P/E series at low frequency respectively. Next we make a plot of δ vs. ϕ (volume fraction) and then fit the experimental data to interpolating splines (Figure 5.38 and 5.39). Through the curve analysis we can find a critical volume fraction ϕ_c at 0.125. At low frequency, when the particle volume fraction is higher than 0.125, the filled polymer systems are elastically dominated. However, at

the volume fraction below 0.125, the filled systems are viscously dominated. So at the critical volume fraction of 0.125, we expect the constant slope of 1 at low frequency for both G' and G''.

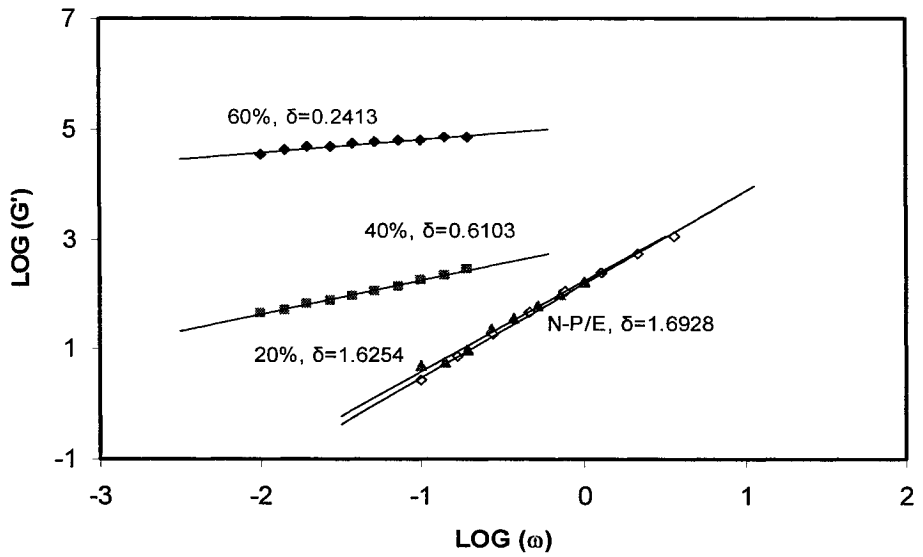

Figure 5.34 Plot of $\log(G')$ vs. $\log(\omega)$ for N-P/E series at low frequency

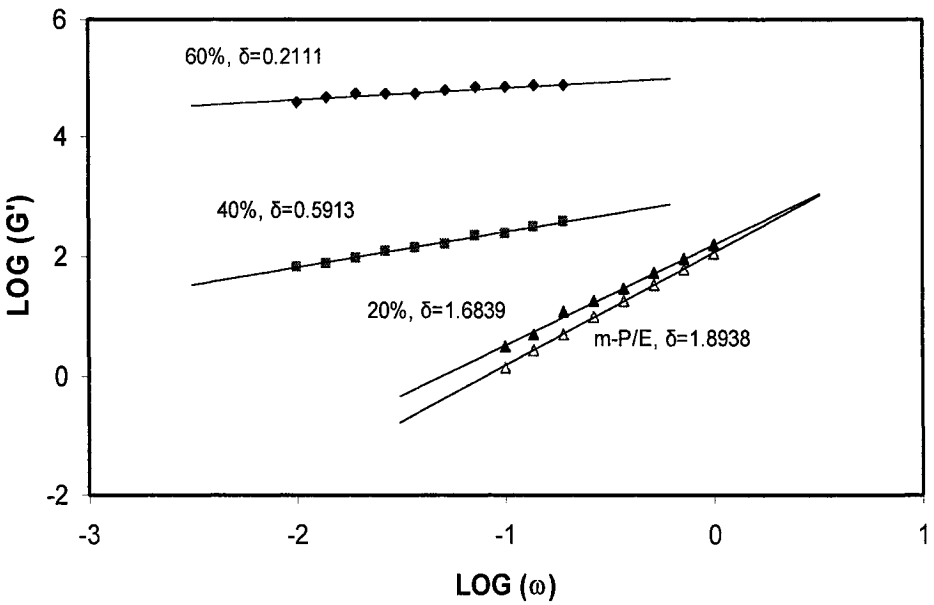

Figure 5.35 Plot of $\log(G')$ vs. $\log(\omega)$ for m-P/E series at low frequency

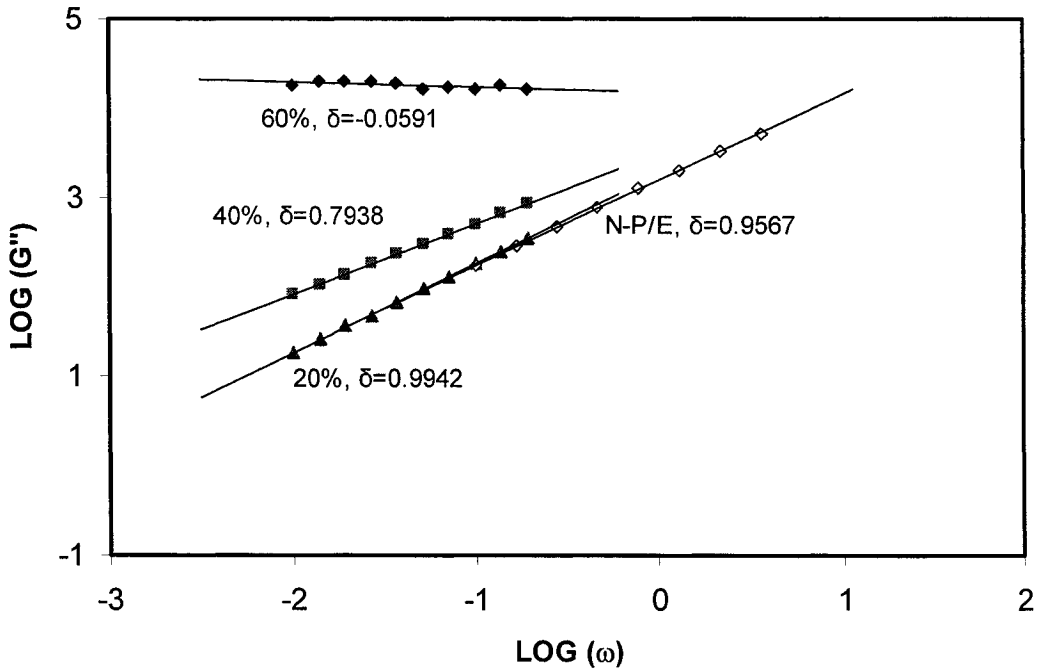

Figure 5.36 Plot of $\log(G'')$ vs. $\log(\omega)$ for N-P/E series at low frequency

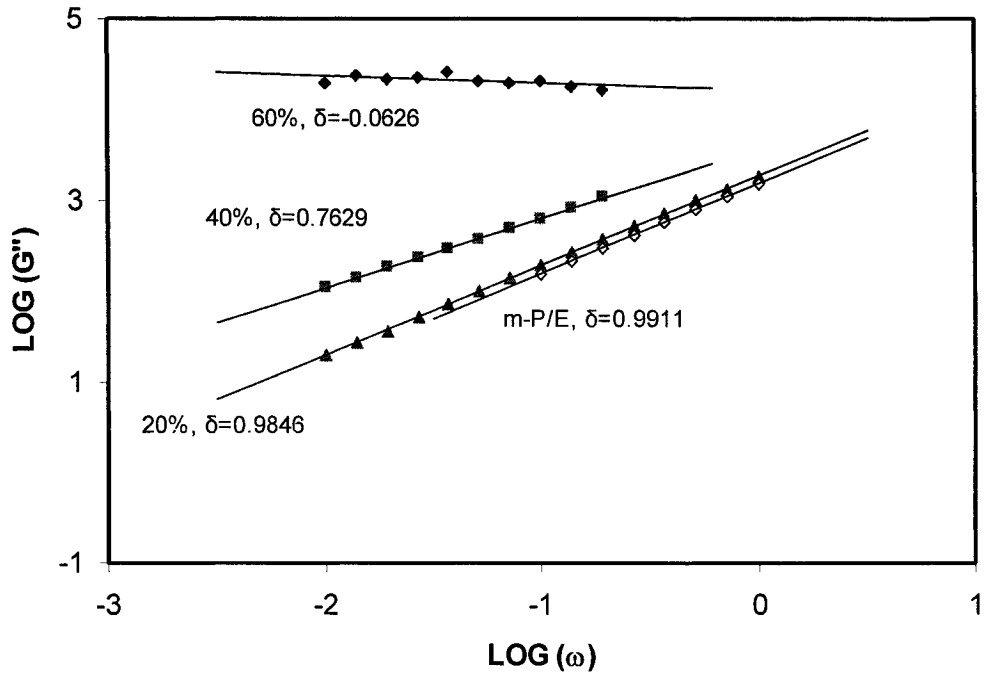

Figure 5.37 Plot of $\log(G'')$ vs. $\log(\omega)$ for N-P/E series at low frequency

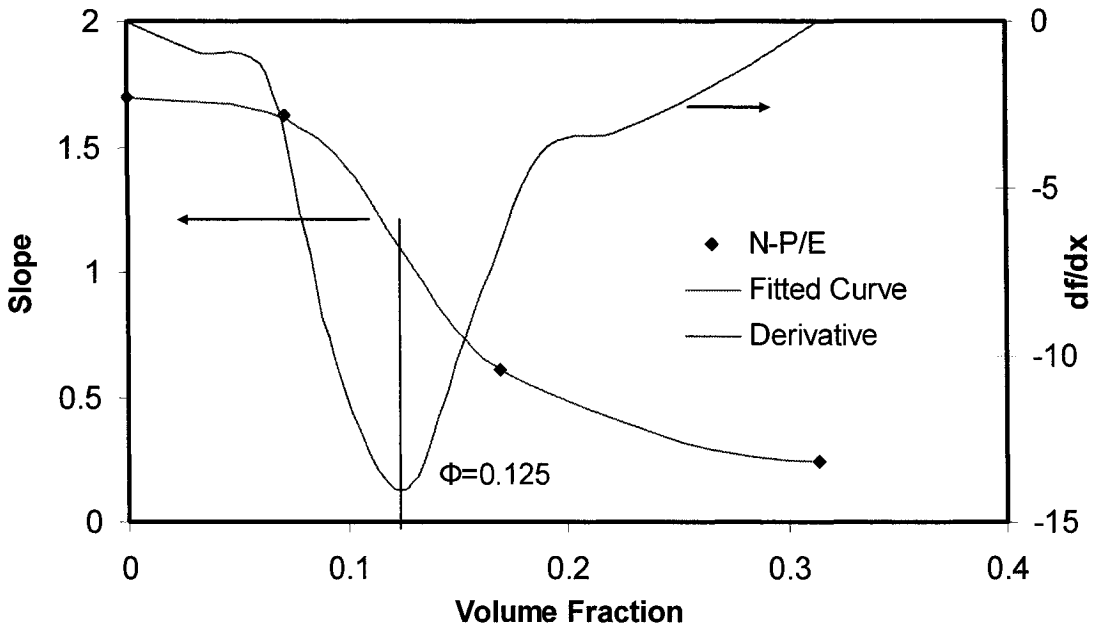

Figure 5.38 Slope analysis of G' for N-P/E series at low frequency

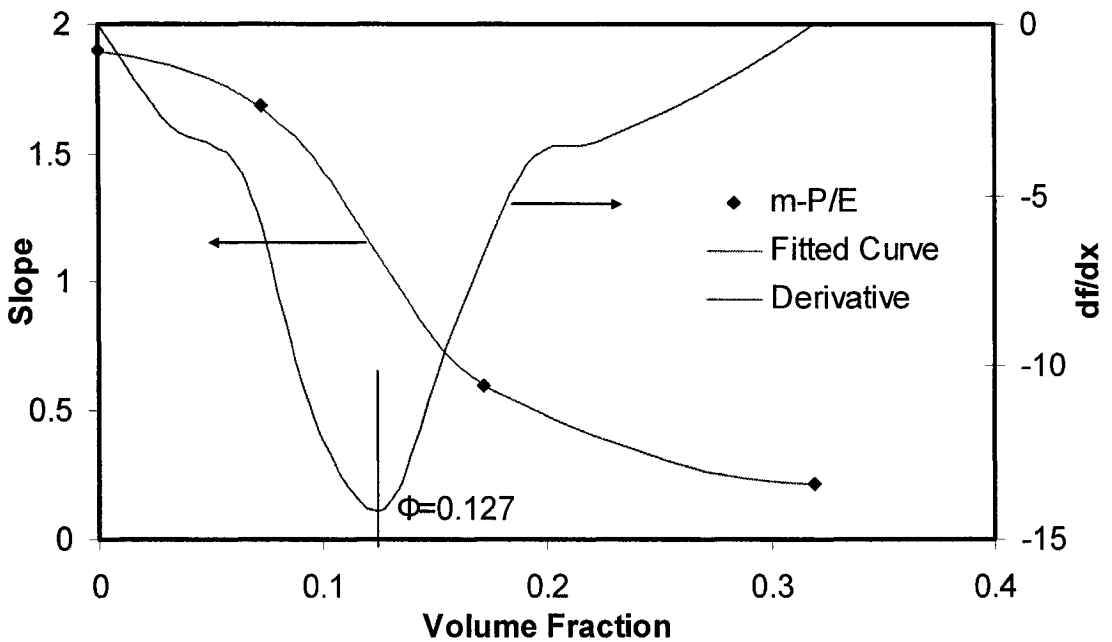

Figure 5.39 Slope analysis of G' for m-P/E series at low frequency

References

1. Wood-Adams, P. M., Costeux, S., *Thermorheological Behavior of Polyethylene: Effect of Microstructure and Long Chain Branching*, Macromolecules 34, 6281-6290, 2001

2. Honerkamp, J., and Weese, J., *A Nonlinear Regularization Method for the Calculation of Relaxation Spectra,* Rheologica Acta, 32, 65-73, 1993

3. Dealy, J. M., Wissbrun, K. F., *Melt Rheology and Its Roles in Plastics Processing: Theory and Applications,* Kluwer Academic Pulishers, 1999

4. D'Orazio, L., Mancarella, C., Martuscelli, E., Sticotti, G., Cecchin, G., Isotectic Polypropylene/Ethylene-co-Propylene Blends : *Influence of the Copolymer Microstructure on Rheology, Morphology, and Properties of Injection-Molded Samples*, Journal of Applied Polymer Science, Vol.72, 701-719, 1998

5. Sakurai, K., *Dynamic viscoelastic properties of poly(ethylene-propylene) diblock copolymer in the melt state and solutions*, Polymer Vol. 37 No. 23, pp. 5159-5163, 1996

6. Lohse, D. J., Garner, R. T., Graessley, W. W., and Krishnamoorti, R., *Miscibility of blends of saturated hydrocarbon elastomers* Rubber Chemistry and Technology; 72, 4, P569, Sep/Oct 1999

7. Choi P., Blom, H. P., Kavassalis, T. A. and Rudin A., *Immiscibility of polyethylene and polypropylene: A molecular dynamics study*, Macromolecules, Vol.28, 8247-8250, 1995

8. Happel, J., and Benner H., *Low Reynolds number Hydrodynamics*, Kluwer Academic

Publishers: Dordrecht, 1991

9. Carreau, P. J., De Kee, D. C. R., and Chhabra, R. P., *Rheology of Polymeric Systems: Principles and Applications,* Hanser/Gardner, 1997

Chapter 6. Conclusions

1. N-P/E exhibits thermorheologically complex behavior which may be caused by the ethylene-enriched molecular chains in the melt. Certain chains congregate at the interface with the particles which leads to a better particle dispersion and enhances interfacial slip under shear flow.
2. N-P/E has a broader molecular weight distribution and chemical composition distribution which cause the bimodal relaxation spectrum.
3. Because of the shear induced particle-particle interaction, all the filled systems have similar time-dependent behavior of viscosity.
4. All the filled systems exhibit a similar shear thinning flow behavior.
5. Because of the stronger interfacial slip in the filled N-P/E, the relative viscosities are much lower than m-P/E series at higher shear stress.
6. N-P/E 20% has a decreasing complex viscosity with time. Due to the lower particle-matrix interfacial adhesion and low filler volume fraction, the free rotation of particles dominates the structure relaxation which causes the better particle dispersion at low filler loading.
7. All the filled systems with higher loadings have similarly increasing complex viscosity in the relaxation process.
8. With the increasing of filler loading, all the filled systems exhibit increasing complex viscosities. Due to the high loadings of particles, N-P/E and m-P/E with 60% loading are solid-like at low frequency.
9. In this work, a simple technique is developed to detect the bulk slip in the viscosity measurement. Thermorheology is used to evaluate the microphase preferences of

different compositions in the melt state. A fitting method is used to quantify the interfacial slip occurring on the particle-matrix interface. These researches are very useful for us to improve the understanding on the rheological behavior of highly filled polymeric systems and also provide some critical information for broadening its application and the necessary data to improve the material properties.

Chapter 7. Future Work

- Study the relaxation mechanism of structured materials (10wt%, 30wt %) to have a further understanding on the Brownian motion of particles and its effect on the rheological properties of the composites
- Steady-state shear viscosity measurements at higher temperatures

  It is necessary to conduct the steady-state viscosity measurements at higher temperature to have a better understanding of the effects of enriched ethylene chains on the viscosities of the composites.
- Study the mechanism of ethylene-enriched phase congregation
- Study the interfacial phenomena by contact angle measurements
- Extensional viscosity measurements to study the particle reorientation in the different flow
- Modeling the rheological behavior to have a theoretical understanding on this low viscosity of the N-P/E composites

Nomenclature

ROMAN LETTERS

AFM Atomic Force Microscopy

b Slip Length

CCD Chemical Composition Distribution

E/O Ethylene Octene Copolymer

E_a Flow Activation Energy

f Fraction of Interfacial Adhesion

$G(t)$ Shear Stress Relaxation Modulus

G' Storage Modulus

G'' Loss Modulus

G_N^0 Plateau Modulus

G^* Complex Modulus

$H(\lambda)$ Relaxation Spectrum

LDPE Low Density Polyethylene

LVE Linear Viscoelasticity

MWD Molecular Weight Distribution

Mw Weight Average Molecular Weight

Mn Number Average Molecular Weight

ODT Order-Disorder Transition

P/E Propylene Ethylene Copolymer

PE Polyethylene

PP Polypropylene

SEM Scanning Electronic Microscopy

T_g Glass Transition Temperature

TTS Time-Temperature Superposition

T Torque

V_θ Velocity Profile

W_{adh} The Work of Adhesion

GREEK LETTERS

a_T Temperature Shift Factor

β Friction Coefficient

β_T Modulus Shift Factor

θ_0 Cone Angle

$\sigma(t)$ Shear Stress

σ_c Critical Stress

γ_{LV} Surface Tension of the Liquid in Equilibrium with its Saturated Vapor

γ_{SL} Interfacial Tension between the Solid and the Liquid

γ_{SV} Surface Tension of the Solid in Equilibrium with its Saturated Vapor

ϕ_a Apparent Volume Fraction

ϕ Volume Fraction

ϕ_{max} Maximum Packing Fraction

ϕ_c Critical Volume Fraction

$\dot{\gamma}_R$ Wall Shear Rate

γ_0 Magnitude of a Step Strain

$\dot{\gamma}(t)$ Shear Rate

$\gamma(t)$ Shear Strain

ω Frequency

δ Phase Angle

λ Relaxation Time

η_r Relative Viscosity

η_0 Zero Shear Viscosity

η^* Complex Viscosity

η' Real Part of Complex Viscosity

η'' Imaginary Part of Complex Viscosity

η_m Medium Viscosity